Energy Efficient Commercial Refrigeration with Carbon Dioxide Refrigerant and Scroll Expanders

Final Technical Report

Recipient:	**TIAX LLC** **35 Hartwell Avenue** **Lexington, Massachusetts 02421-3102** **U.S.A**
Principal Investigator:	**John Dieckmann**

Project Title:	**Energy Efficient Commercial Refrigeration with Carbon Dioxide Refrigerant and Scroll Expanders**
Work performed under Award No.:	**DE-EE0003922**
Area of Interest 5:	**Water Heating, Residential and Commercial Appliances and MELS**
Technical Sub Topic 5.3:	**Commercial Appliances**
Date:	**April 04, 2013**

Table of Contents

List of Tables

List of Figures

1.0 Introduction

1.1 Backgound

Commercial refrigeration systems consume an estimated 0.91 quads of primary energy annually. Approximately 0.33 quads of this is consumed in the large centralized refrigeration systems used in supermarkets. In the late 1980s and early 1990s, significant progress was made by the industry in improving the efficiency of these systems. Innovations such as uneven parallel compressors for capacity modulation, floating head pressure control, improved display case thermal insulation and glass doors, and demand defrost were adopted. A new, higher efficiency generation of heavy duty semi-hermetic reciprocating compressors was introduced at this time. However, efficiency gains have plateaued in recent years; new options are needed.

Current supermarket refrigeration systems are built around conventional fluorocarbon refrigerants – HFC-134a and the HFC blends R-507 and R404A, which replaced the CFC refrigerants, R-12 and R-502, respectively, used prior to the Montreal Protocol phase out of ozone depleting substances. While the HFC refrigerants are non-ozone depleting, they are strong greenhouse gases, so there has been continued interest in replacing them, particularly in applications with above average refrigerant leakage. Large supermarket refrigeration systems have proven to be particularly difficult to maintain in a leak-tight condition. Refrigerant charge losses of 15% of total charge per year are the norm, making the global warming impact of refrigerant emissions comparable to that associated with the energy consumption of these systems.

Considerable interest has been focussed on so-called "natural" refrigerants, particularly carbon dioxide, which is non-flammable, low in toxicity, and low in cost. For cooling applications rejecting heat to outdoor air, using carbon dioxide as the refrigerant entails a transcritical refrigeration cycle, because often the heat must be rejected at a temperature above the 88°F critical temperature. The practical impact of this is that operating pressures are quite high and the theoretical thermodynamic cycle COP is low. The low COP is offset to a degree by superior transport properties of carbon dioxide, but the simple transcritical cycle is less efficient than conventional vapor compression cycles. In an SBIR program for the U.S. Army[1], TIAX showed that by expanding the high pressure CO_2 refrigerant to the evaporator pressure with a work recovery expander, a CO_2 based transcritical system can provide comparable efficiency to a conventional fluorocarbon refrigerant based vapor cycle at the stringent rating conditions for military air conditioning equipment. In subsequent analysis, we found that with a scroll expander used in a transcritical CO_2 cycle for commercial refrigeration, the inherent thermodynamic cycle efficiency can be *improved* compared to a conventional state-of-the-art vapor compression cycle. Combined with other potential performance advantages of CO_2, significant energy savings relative to the current state-of-the art are possible.

A transcritical CO_2 based DX type supermarket refrigeration system with a scroll expander is shown schematically in Figure 1-1. It adopts the currently commonplace configuration of rack mounted, uneven parallel compressors. A rack of compressors typically has enough capacity to handle many refrigerated or frozen food display cases. As shown in Figure 1-1, a two-stage system is used, with an upper stage that operates at 35^o – 45^oF low side pressure (comfortably below the 88^oF critical temperature of CO_2) and a high side pressure where heat is rejected to

ambient. The lower stage is a conventional (except for the CO_2 refrigerant), rack-mounted parallel, compressor system. At the interface between the lower and upper stages, the CO_2 liquid and vapor exiting the scroll expander enters a refrigerant receiver where the liquid and vapor are separated. The vapor is returned to and compressed by the upper stage compressor, along with vapor from the lower stage compressors; the liquid is sent to the refrigerated/frozen display cases.

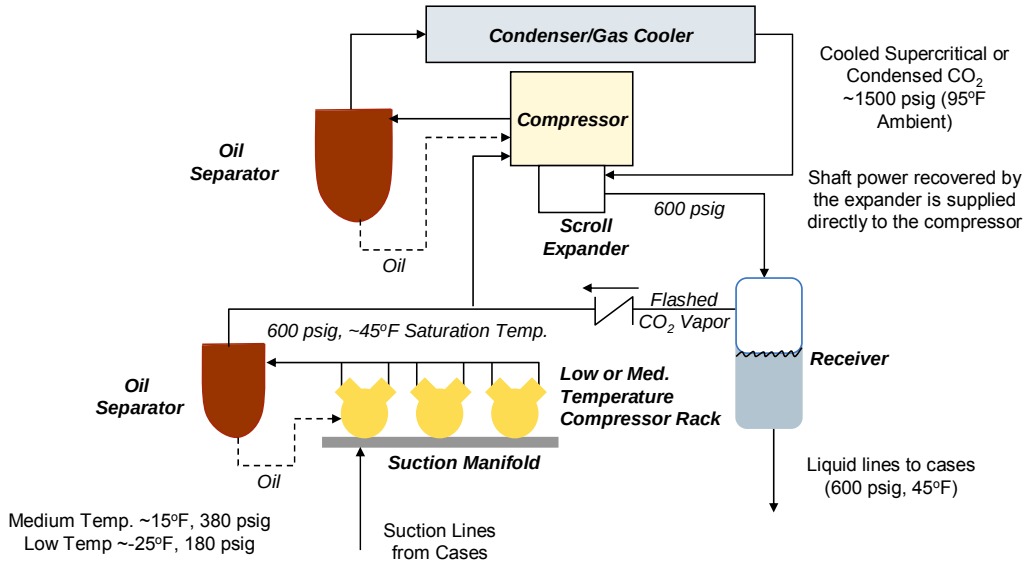

Figure 1-1: Commercial Refrigeration System Design for CO_2 Refrigerant with Scroll Expander(s)

The cycle is shown on a P-h diagram for medium and low temperature applications in Figure 1-2.

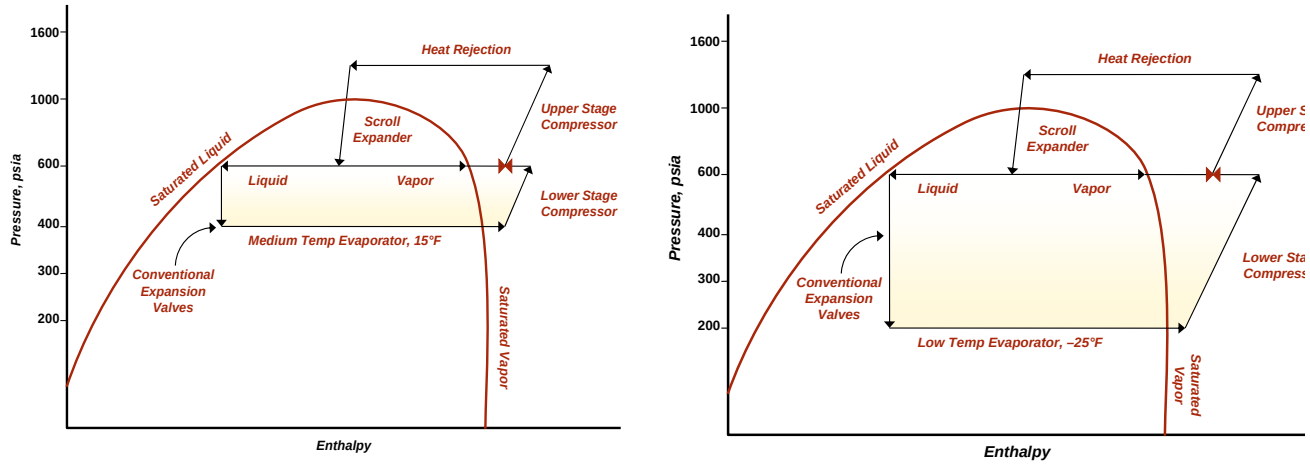

Figure 1-2: P-h Diagrams for Medium and Low Temperature Refrigeration

The factors that provide the potential for energy savings (also see Table 1-1) are:

- A work recovery expander and a flashed vapor economizer at the intermediate stage that more than offset the inherent transcritical CO_2 energy disadvantage. Analysis shows that the proposed CO_2 based system uses 10% less energy at low temperature and 5% less energy at medium temperature, based on the thermodynamic cycle alone.

- Suction line pressure losses are negligible with high pressure CO_2, while in fluorocarbon refrigerant based systems, suction line pressure losses amount to 5°F or more in reduced saturation temperature at the compressor inlet, increasing compressor power by at least 5%.
- Head pressure control is not needed until the ambient temperature is lower than 25°F. In conventional systems, head pressure control maintains a minimum 80°F condensing temperature to provide a high enough liquid refrigerant pressure to flow through expansion valves. In the CO_2 based system, the head pressure control setting is approximately 40°F, corresponding to an outdoor temperature of 20-25°F. Approximately 4000-5000 hours of operation at lower condensing temperatures saves, conservatively, 15% annually.
- Low pressure ratio improves compressor efficiency about 5%.
- Better refrigerant side heat transfer – the transport properties of CO_2, combined with microchannel heat exchangers enables evaporating temperatures to increase by 2-3°F.

Table 1-1: Summary of Estimated Efficiency Improvements

Factor	Δ Efficiency	
	Low Temperature	Medium Temperature
Thermodynamic Cycle	+10%	+5%
Reduced Suction Line Pressure Drop	+5%	+5%
Lower Ambient Temperature for Head Pressure Control Cut-in	+15%	+15%
Improved Compressor Efficiency	+5%	+5%
Increased Evaporator Temperature	+5%	+5%
Total	**+40%**	**+35%**

It is noteworthy that the efficiency improvement in a transcritical CO_2 cycle that is provided by a work-recovery expander is delivered to the overall cooling system by two primary paths – putting the recovered work (mechanical power) to good use and by the increased refrigeration effect provided by the removal of the expansion work from the CO_2. Roughly 60% of the improvement is attributable to useful mechanical power recovery and 40% to the increased refrigeration effect. Thus, it is critical for the recovered expansion work to be put to good use. In most instances, the best option is to feed the recovered expansion power to the compressor shaft, as we plannned to do in this program. This enables the expander to "piggy-back" off of the compressor shaft and housing, minimizing the added hardware involved in implementation and allowing the expansion shaft power to be utilized without any additional conversion losses.

Beyond the value of the energy savings, there are compelling reasons why CO_2 will be attractive for commercial refrigeration.

- CO_2 is a low cost refrigerant ($100/metric tonne in bulk, 95% less than HFC blends), both for the initial system charge and leakage replacement
- Environmentally benign – Zero ODP and GWP, translates into *cost* advantages:
  - Not subject to any of the no-vent type regulations, reducing maintenance costs
  - No CAAA refrigerant reporting/emission compliance issues with CO_2,
- High pressure and high density translates into smaller (half the diameter) and lower cost refrigerant lines, more compact compressors and heat exchangers

- A smaller condenser is needed, reducing the size and cost by approximately one-third.

While any type of expander with the assumed 70% efficiency would provide the efficiency/COP levels estimated above, there are unique attributes of a scroll expander that offer several system advantages for an integrated CO_2 compressor and expander:

1. The scroll expander is compact and has few parts. The added weight and volume to accommodate the expander is less than 10% of the motor-compressor weight.
2. Self-porting assures that the correct amount of high pressure CO_2 refrigerant is admitted and the correct discharge timing occurs without intake or discharge valves.
3. The scroll is readily integrated with common compressor types (direct shaft connection and common lubrication system); the shaft power recovered by the expander can be supplied directly to the compressor.
4. With proven ability to handle two-phase flows, the scroll expander can operate at design ambient and with liquid and vapor at lower outdoor temperatures.
5. The efficiency level of 70-75% is attainable with conventional CNC machining tolerances, based on extensive TIAX analysis, confirmed with in-house leakage testing and in-house testing of initial scroll expander prototypes.

The TIAX Scroll expander technology utilizes a geometrically simple, low parts count design to provide a robust, efficient expander that operates well in the challenging conditions (especially the high pressures and pressure differences) of CO_2 refrigeration cycles. We have previously developed two initial prototype expanders, one aimed at small, electric motor driven air conditioning systems (in the aforementioned Army SBIR project) and one aimed at automobile air conditioning. Shaft power basis isentropic efficiency greater than 70% has been measured with both of these prototypes. In the Army project, an integrated compressor (a two-stage rotary compressor) and scroll expander was developed which exhibited high mechanical efficiency, but showed the need for more effective thermal isolation between the warm compressor and the cooler expander.

For the supermarket refrigeration application, a larger scale expander is needed and it must be integrated with a heavy duty semi-hermetic compressor used for supermarket refrigeration application. A mechanically robust and efficient interface that provides sufficient thermal isolation between the compressor and expander must be provided. The program addressed these challenges.

1.2 Project Objectives

In this program, TIAX undertook a proof of concept development of the key component for CO_2 commercial refrigeration, the scroll expander integrated with a CO_2 compressor that is suitable for application in a supermarket refrigeration system. In Phase I, TIAX designed, fabricated, and tested the scroll expander. The design anticipated the integration of the expander with the compressor in Phase II. Phase II involved fabrication of the integrated system and testing it under conditions representative of those found in supermarkets.

Goals The goals of this project were to (1) reduce the energy consumed by commercial refrigeration systems and (2) reduce the greenhouse gas effects resultant from the release of

fluorocarbon refrigerants to the atmosphere. Associated with (1) is also a reduction in greenhouse gasses due to reduced electricity usage.

Objectives TIAX pursued the above goals in this project by further developing and demonstrating a novel work recovery expander technology that enables the cost effective use of CO_2 as a refrigerant. The specific objectives were to:

- Develop a scroll CO_2 expander with an isentropic efficiency of 75% at design conditions
- Integrate the expander with a semi-hermetic CO_2 compressor

2.0 Commercial Refrigeration Design Study

A key objective of the commercial refrigeration system design study was to determine the capacity of the TIAX scroll CO_2 expander that would match with the range of compressor capacities likely to be used in a transcritical stage of a CO_2-based supermarket refrigeration system. Based on review of transcritical CO_2 compressor product literature, discussions with IR-Hussmann engineers, and analysis, we decided to size the expander to be matched with a compressor having a nominal capacity comparable to a nominal 15 horsepower refrigeration compressor. This falls roughly in the middle of the range of typical capacities – a complete product family would be covered by a modest +/- 50% capacity scaling range. The CO_2 mass flow rate will be on the order of 1,500 lb/hour and refrigeration capacity of approximately 60,000 Btu/hr for low temperature or 90,000 Btu/hr for medium temperature would be provided.

A second objective of the task was to refine the system performance analysis and compare projected performance to both cascade and conventional supermarket systems. Figures 2-1 and 2-2 plot COP vs. gas cooler leaving temperature for the TIAX 2 stage with expander all CO_2 system, for medium and low temperature, respectively. Figures 2-3 and 2-4 plot COP vs. R404A condensing temperature for the R404A – CO_2 cascade system, for medium and low temperature, respectively. For a given outdoor temperature the R404A condensing temperature will be approximately 10°F higher than the gas cooler leaving temperature of the transcritical system. Taking this into account when comparing COPs, the transcritical + expander cycle compares favorably to the R404A – CO_2 cascade system.

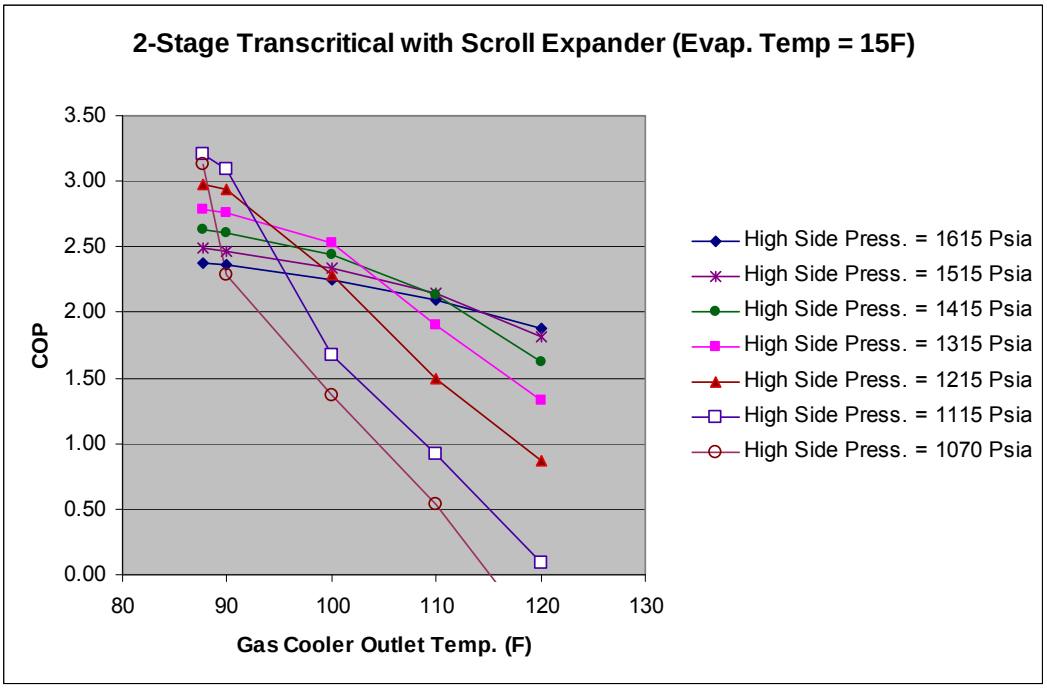

Figure 2-1: COP vs. Gas Cooler Leaving Temperature for TIAX 2 Stage with Expander All CO_2 System for Medium Temperature (evaporating temperature 15°F)

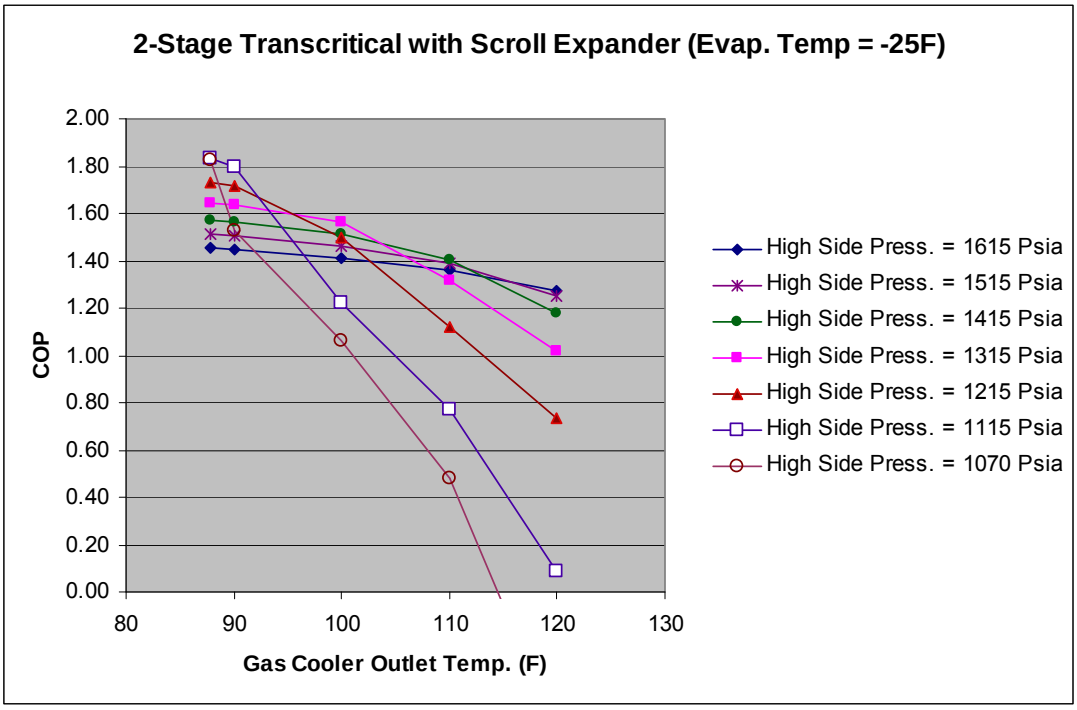

Figure 2-2: COP vs. Gas Cooler Leaving Temperature for TIAX 2 Stage with Expander All CO_2 System for Low Temperature (Evaporating Temperature -25°F)

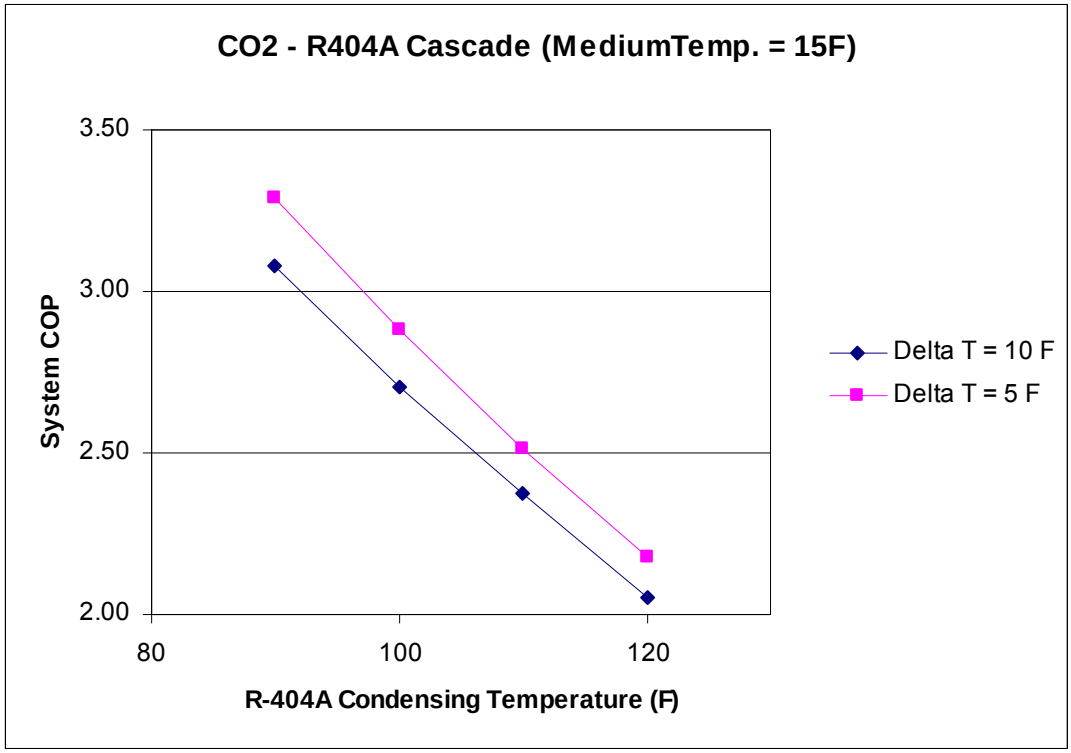

Figure 2-3: COP vs. Condensing Temperature for CO_2 – R404A Cascade System for Medium Temperature (Evaporating Temperature 15°F)

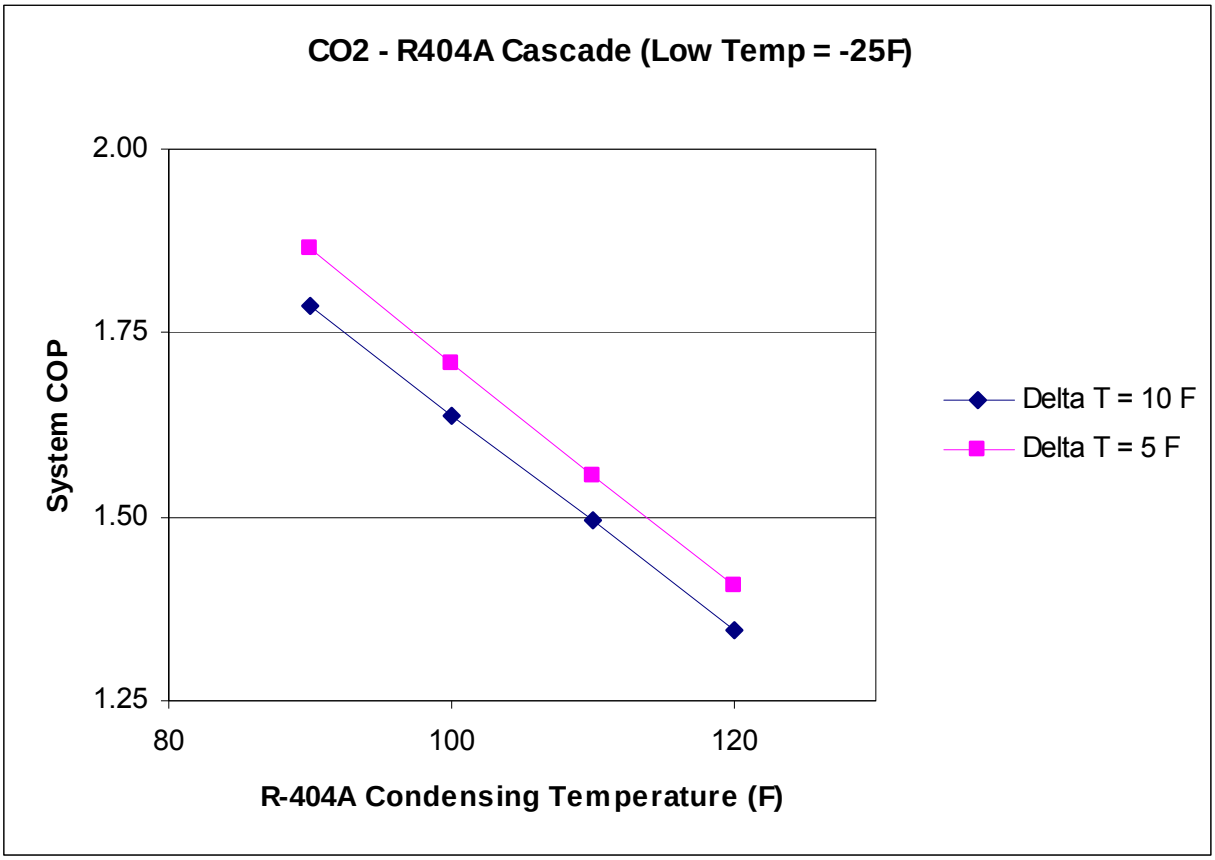

Figure 2-4: COP vs. Condensing Temperature for CO_2 – R404A Cascade System for Low Temperature (Evaporating Temperature -25°F)

Figure 2-5 plots the COP of the TIAX 2 stage with expander all CO_2 system vs high side pressure for several gas cooler leaving temperatures. Superimposed on these plots is two lines showing where the system would operate at two fixed compressor inlet to expander inlet displacement ratios – in both cases, as the outdoor temperature and the resulting gas cooler leaving temperature varies, the high side operating pressure stays close to the level where the maximum COP is obtained.

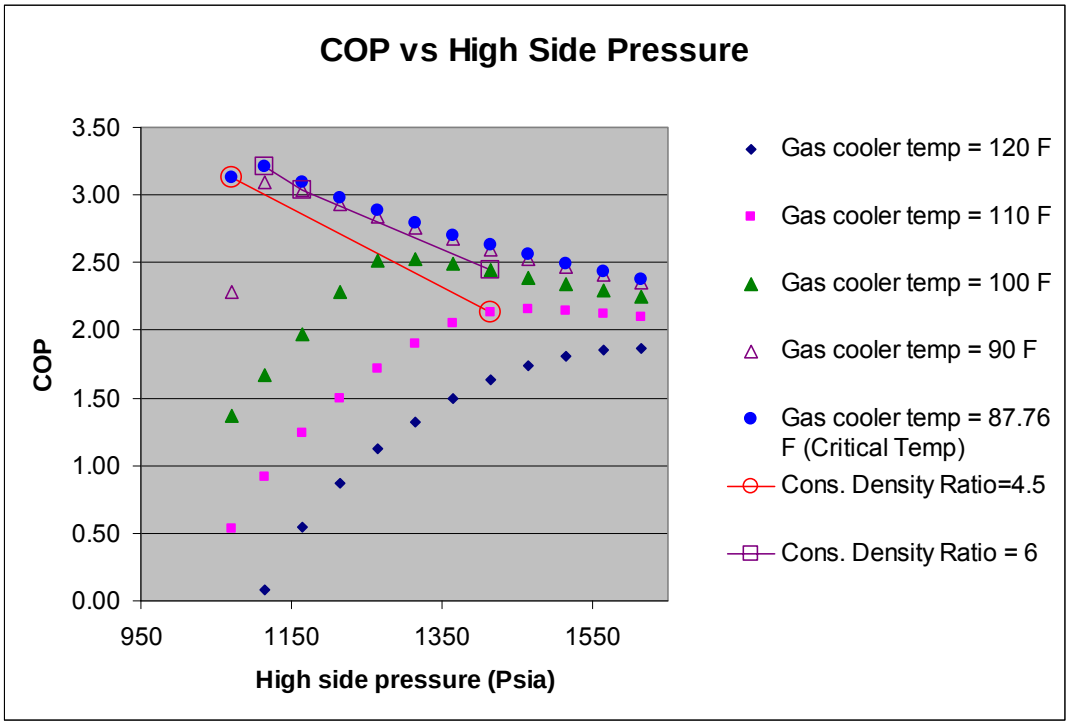

Figure 2-5: High Side Pressure vs. Gas Cooler Leaving Temperature with Fixed Displacement Scroll Expander and Fixed Displacement CO_2 Compressor On A Common Shaft

3.0 Expander Design

3.1 Design of the Integrated Compressor and Expander

An initial design of the integrated compressor and expander was completed early in the program. This layout level design included the expander design details and an interface with a generic semi-hermetic reciprocating transcritical CO_2 compressor. The layout includes a thermal barrier between the relatively warm compressor and the cooler expander, intended to limit compressor to expander heat conduction to less than 10% of the mechanical power recovered by the scroll expander. The thermal barrier is a ribbed hollow spool fabricated from relatively low thermal conductivity 304 stainless steel. The barrier piece also includes a shaft seal and a shaft bearing. Further work on the integrated compressor and expander design was postponed until the POC expander test results had either verified the design or pointed the way to necessary modifications to the expander design.

3.2 Proof of Concept Expander Design

In the first quarter of the program, the scrolls were sized, a layout drawing was completed, the lubrication and oil level control scheme was developed, and bearing sizing calculations were completed. The thermal barrier was incorporated into this prototype design so that its effectiveness could be evaluated experimentally before committing it to the integrated compressor and expander.

3.3 Supporting Analysis of the Expander Design

The design of the expander was supported by analysis in the following areas:

- The lubrication and oil level control scheme
- Bearing sizing calculations
- Thermal conductance of the thermal barrier
- Pessure loading on the scroll parts
- Finite element analysis of stresses and deflections of the scroll parts

The lubrication and oil management system for the POC expander prototype is shown in Figure 3-1. The high pressure CO_2 leaving the compressor passes through an oil separator before moving on to the gas cooler and the expander. Oil collected in the oil separator has three paths, ultimately back to the Dorin compressor inlet, which passes into the compressor crankcase and oil sump. For expander lubrication, oil is introduced to the oil sump of the expander orbital drive by a solenoid valve controlled by an optical level sensor. The oil feed makes up for oil gradually leaving the expander orbital drive via the main crankshaft bearing and the thrust bearing oil seal. Within the expander orbital drive, splash lubrication distributes oil to the orbiting scroll thrust bearing and drive bearing, the Oldham coupling, and the main drive shaft bearing. A second path provides a slow oil bleed through a small needle type metering valve to lubricate the ball bearing and shaft seal at the output shaft end. A third path provides a slow bleed of oil back to the compressor inlet.

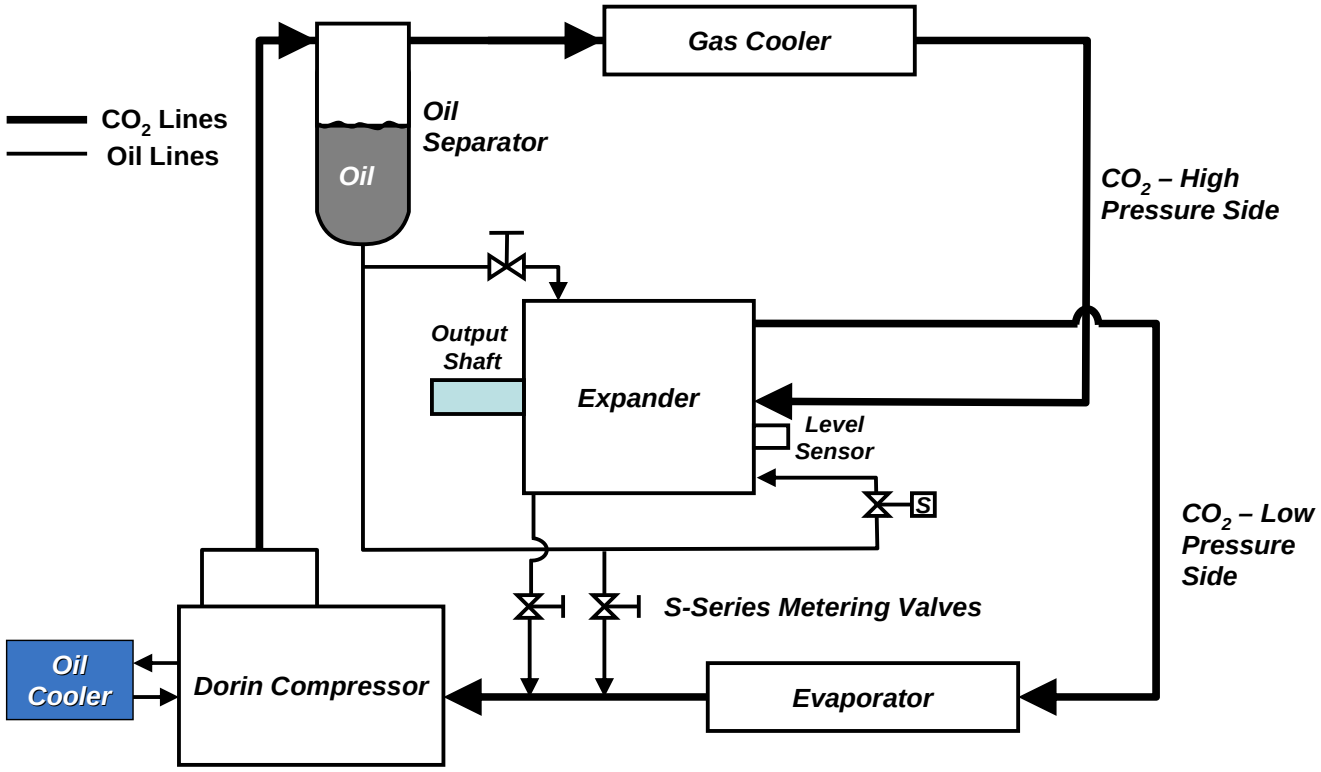

Figure 3-1: Lubrication and Oil Management for the POC Scroll Expander Prototype

The orbital drive mechanism for the expander includes a drive shaft supported by two bearings and an eccentric (to the shaft centerline) bearing that is driven by the orbital motion of the scroll, in turn driving the rotation of the drive shaft. The eccentric drive bearing and the shaft bearing closest to the orbiting scroll are hydrodynamically lubricated sleeve bearings. This type of bearing was selected for the long, wear-free service life that can be obtained with properly sized hydrodynamic bearings.

These two bearings were sized using the procedure in [CBBI, 1971]. Based on the bearing diameter (D), length (L), clearance with the shaft, speed, load, and lubricant absolute viscosity, a bearing characteristic number is calculated, essentially the inverse of the classic Sommerfeld number. From the bearing characteristic number and L/D, the eccentricity ratio is found on a chart and the frictional power factor is found on a second chart. The minimum oil film thickness is (1-eccentricity ratio)(radial clearance) and the friction power loss is the product of the frictional power factor, clearance ratio, diameter, speed and load. Table 3-1 summarizes the calculations, with loads on the bearing estimated for the expected maximum power output of the expander of 3 horsepower. For both bearings the minimum oil film thickness is greater than 300 microinches, which is ample separation between the shaft and the sleeve to prevent any wear. The total friction power loss for the two bearings is approximately ¼ horsepower, 8% of the expander power output.

Table 3-1: Hydrodynamic Sleeve Bearing Calculations for the Expander Orbital Drive Mechanism

	Eccentric Drive Bearing	*Shaft Bearing*
Diameter (inches)	1.75	1.25
Length (inches)	0.75	1.00
Clearance factor	1.5	1.5
Speed (RPM)	1,800	1,800
Load (lbf)	700	800
Absolute Viscosity (centipoise)	60	60
Bearing Characteristic Number	0.00476	0.0107
Eccentricity ratio	0.72	.59
Minimum film thickness (microinches)	351	384
Friction power factor	0.045	.035
Friction power loss (horsepower)	0.15	0.95

Detailed analysis of the scroll pocket areas, the gas (CO_2) pressure during expansion, and the resulting axial gas pressure force acting to deflect the scrolls was done and the resulting forces used as input to a finite element analysis of the stress and axial deflection of the scrolls. Figure 3-2 shows the FEA results for the orbiting scroll under maximum pressure loading. The center deflects by about 0.00015 inches, a small enough deflection that the internal sealing between the two scrolls will not be compromised significantly.

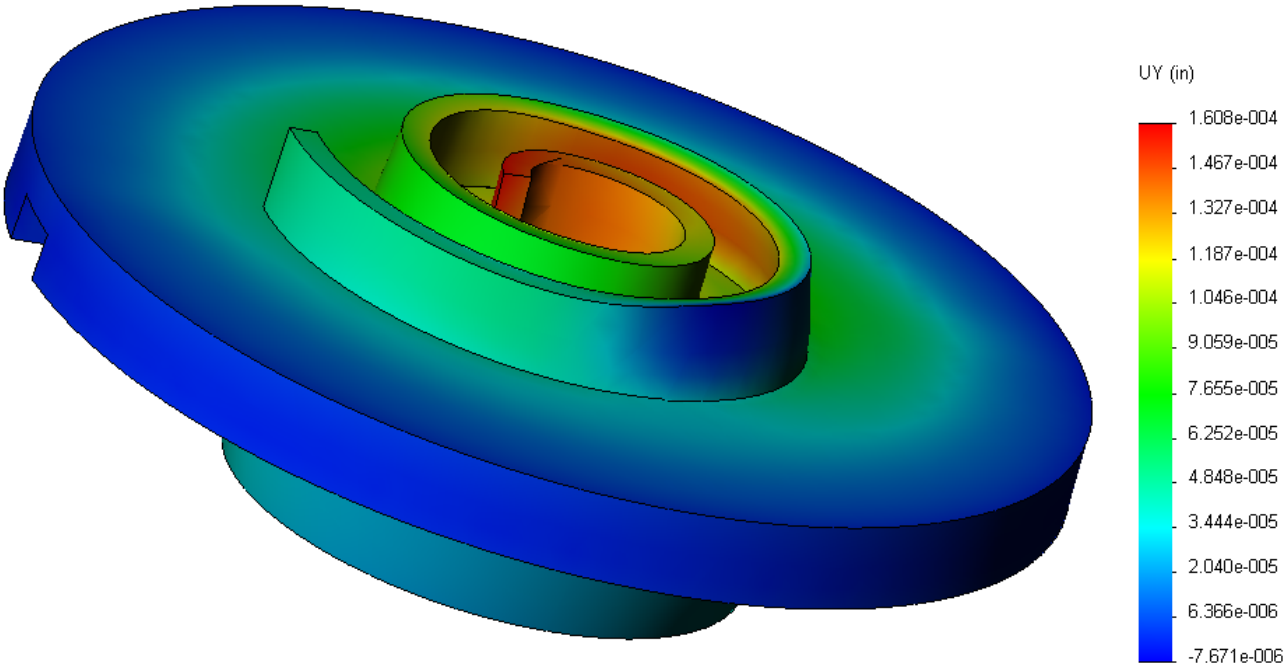

Figure 3-2: FEA Result Showing the Axial Deflection of the Orbiting Scroll Under Maximum Pressure Loading

The thermal conductance of the thermal isolation spool was calculated based on the cross sectional area and length of the spool piece and the thermal conductivity of stainless steel:

Conductance = (9.4 Btu/hr-ft-^{o}F) X (5.46 in^{2}/2.75 inch) X (ft/12 inch)

= 1.55 Btu/hr-^{o}F

With the maximum anticipated temperature difference between the motor and the expander orbital drive of 100^{o}F, the heat conduction through the spool would be 155 Btu/hr.

4.0 Expander Fabrication

Beginning with the detailed design of the expander, fabrication followed 4 basic steps – purchasing material and standard parts, machining parts, inspection of parts, with any necessary rework, and assembly. The materials that were purchased were:

- Durabar 65-45-12 ductile iron round bar stock for the two scrolls.
- Type 304L stainless steel round bar stock for the thermal isolator
- 6061-T6 aluminum for the Oldham coupling
- 1018 steel round bar stock for most other parts

The scroll parts were machined in the TIAX CNC machining center, several of the larger parts were machined at outside vendor machine shops and several of the smaller parts in-house at TIAX.

Figure 4-1 is a photograph of the internal parts laid out in an exploded view. Figure 4-2 is a photograph of the main housing. The major fabricated parts for the expander are:

- Main housing
- Fixed and orbiting scrolls
- Oldham coupling -- moving and stationary rings
- Drive shaft
- Thermal isolation spool/main bearing support
- Scroll eccentric drive bushing
- Shaft output end cap
- Oil level sensor housing
- CO_2 inlet and outlet tubes
- Scroll end cover plate
- Counterweight and trim weight

The major purchased parts for the expander are:

- Oil level sensor
- DU bearings for orbiting scroll drive bearing and drive shaft main bearing
- Ball bearing for drive shaft output end bearing
- Sight glasses
- O-rings
- Fasteners
- Radial preload spring for scroll drive bushing

Figure 4-1: Fabricated Parts of the Scroll Expander

Figure 4-2: Main Housing

Dimensional inspection of completed parts focused on close tolerance dimensions that are critical to the assembled fits and alignment. Most of these dimensions were within tolerance. The few exceptions to this were corrected in our machine shop.

The most important dimensions relating to the expander performance are of the scroll surfaces, particularly the axial dimensions – the flatness of the plane defined by the scroll tip surface and the height from the scroll tip surface to the scroll base. The flatness of the fixed scroll tip plane, which extends to the thrust bearing outside of the actual scroll contours, was within 0.0002 inch (2 ten-thousandths of an inch) and the height was consistently within less than 0.0001 inch of 0.5001 inch. The flatness of the orbiting scroll tip plane was within 0.0002 inch and the height was consistently within less than 0.0001 inch of 0.5001 inch. The outer area of the base plane of the orbiting scroll, which is the mating thrust bearing surface with the thrust bearing area of the fixed scroll, is dished upward slightly, by 0.0003 to 0.0004 inches. This could cause the axial clearance between the two scrolls to be somewhat larger than ideal, but is potentially acceptable because the aforementioned height dimensions where held as closely as they were and under pressure loading the slight dishing may deflect toward flattening out. This area could be flattened by lapping the outer base plane area, but we opted to operate the expander first and evaluate the initial test results.

The key assembly and initial check-out steps of the expander prototype steps are:

- Subassembly dimensional inspection
- Pressure testing the housing assembly

Subassembly dimensional inspection was focussed in the critical fit areas:

- Fit of the housing to the ball bearing outer race at the outer, shaft seal end of the shaft. The required fit is an interference fit of 0.0010 inch. The actual bearing outer race outside diameter and the as machined housing bore resulted in an interference of 0.002 inches, so the housing bore was increased to obtain the correct interference.
- Fit of the shaft to the ball bearing inner race at the outer, shaft seal end of the shaft. The shaft diameter was a few ten thousandths of an inch large for the required transitional slip fit, so the shaft diameter in this area was carefully reduced to obtain the correct fit.
- Clearance between the shaft and the main shaft sleeve bearing was initially a slight interference. This is a hydrodynamic sleeve bearing whose diametral clearance should be between 0.001 and 0.002 inches. The shaft diameter was reduced in this area to obtain the correct clearance
- The total axial clearance for the orbiting scroll and Oldham coupling ring between the fixed scroll and the stationary Oldham ring was custom fit to between 0.002 and 0.003 inches, to limit the maximum axial clearance between the two scrolls at start up to a small amount.
- The fit of the eccentric drive bushing with the drive bearing on the back of the orbiting scroll. This is a hydrodynamic sleeve bearing whose diametral clearance should be between 0.002 and 0.003 inches. The actual fit was found to be within this range

- The perpendicularity and concentricity of the axis of rotation of the assembled shaft in the housing to the shoulder and pilot diameter in the housing that locate the fixed scroll. Perpendicularity was within 0.002 inch over an 8 inch diameter, or within 1/4 of a milliradian of perpendicular. Concentricity was within 0.004 inches radially. Both of these are well within the range that the radially compliant drive can accommodate.

The housing assembly – housing, end covers, shaft, shaft seal, and static O-ring seals – was leak tested and pressure tested. A dial indicator was placed on the center of the end cover to measure the deflection under pressure. The pressure was increased in increments of 500 psi and returned to zero, to see if any plastic deflection had occurred. At 2000 psi, plastic deformation was first observed, so the housing is safe for pressures up to 1300 psi (150% of 1300 psi <2000 psi), 200-300 psi higher than anticipated housing pressures.

Then the expander was assembled and installed in the test loop for development testing.

5.0 Expander Testing

5.1 Test Loop

A schematic of the test loop for the POC expander prototype is shown in Figure 5-1. At the beginning of the project, space for the Scroll CO_2 expander test loop was assigned in the TIAX "Flex Lab" and heavy duty lab benches were located in this space. Installation of the variable frequency drives (VFDs) for the transcritical compressor power input and the expander output speed control motor was completed. Figure 5-2 is a photograph of the VFD installation.

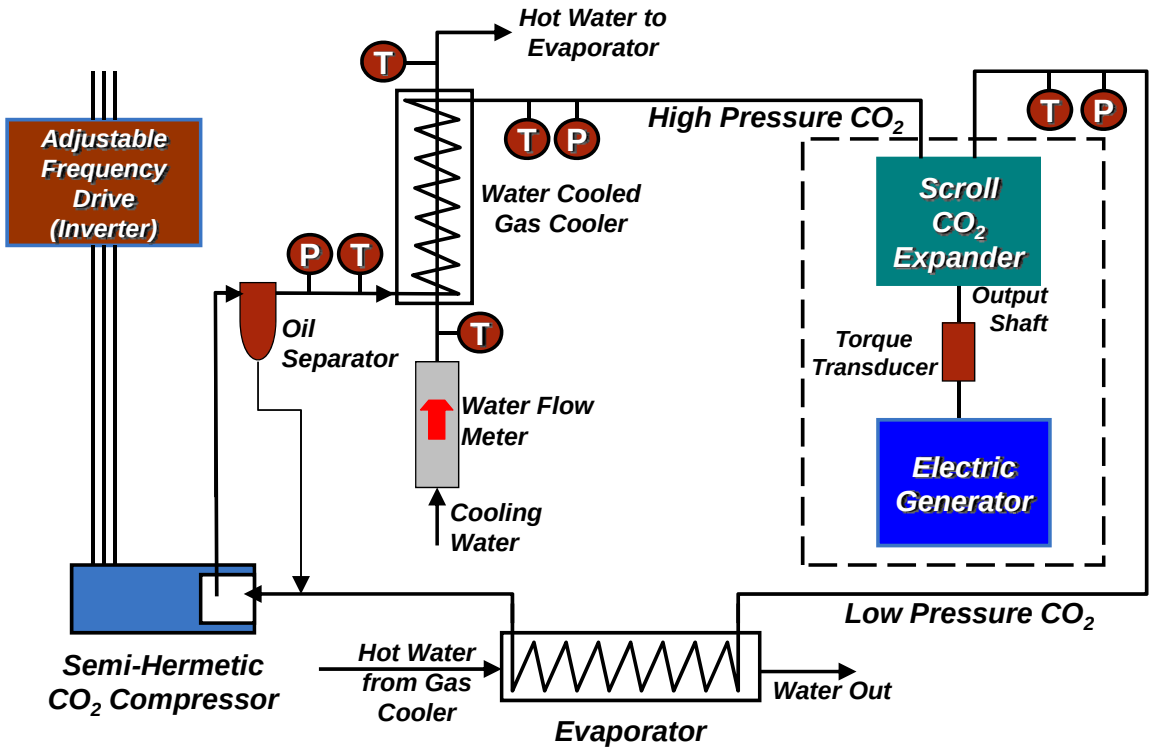

Figure 5-1: Schematic of Test Loop for the POC Expander

Figure 5-2: VFDs for CO_2 Expander Testing

Sizing calculations for the water-cooled gas cooler and water-heated evaporators were completed. To allow the use of readily available stainless steel tubing, each of these heat exchangers is a coiled shell and tube configuration. The shell is 25 feet long, with seven 3/8 OD stainless steel tubes in the shell. The high pressure CO_2 is on the tube side and water is on the shell side. These heat exchangers have been completed and pressure tested to 3,000 psi (50% over the maximum working pressure of the high pressure side of the system. Figure 5-3 is a photograph of the CO_2 tube header that was made for pressure testing. It was tested to 5,500 psi without any failure, well above the 2,000 psi maximum working pressure. Figure 5-4 is a photograph of these heat exchangers and Figure 5-5 shows the heat exchangers where they are located in the test loop, with the cooling/heating water plumbing attached.

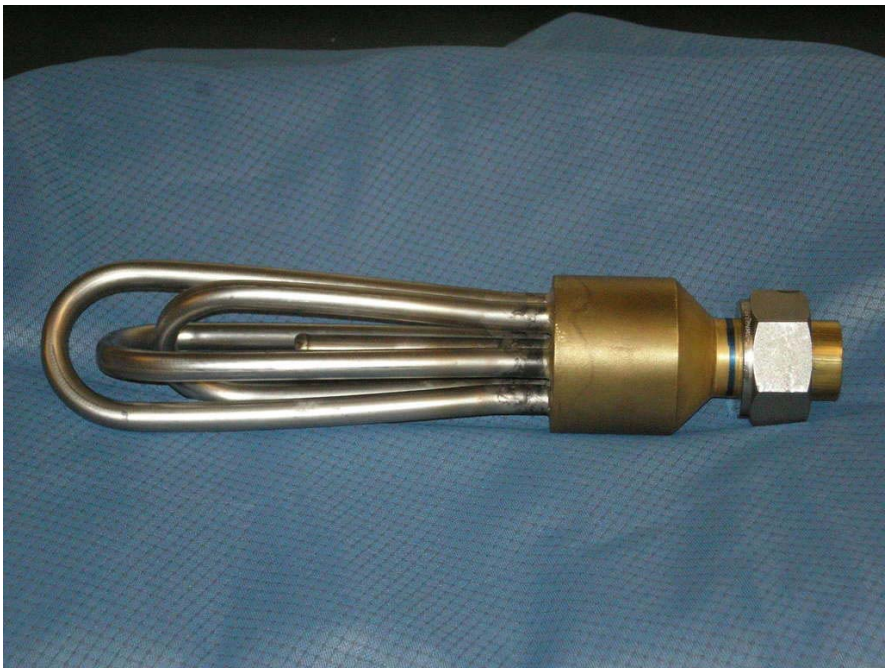

Figure 5-3: Pressure Test Article of the CO_2 Header for the Gas Cooler and Evaporator

Figure 5-4: Completed CO_2 Gas Cooler and Evaporator (the Gas Cooler is on Top of the Evaporator)

Figure 5-5: CO_2 Gas Cooler and Evaporator in the Test Loop with CO_2 Piping

Figure 5-6 shows the cooling water plumbing – the left most line goes to drain, hot and cold supply lines next to the drain line are connected to the temperature and flow control valve. The line leaving the temperature-flow control valve goes to the rotameter type flow meter, after which the water goes to the water inlet to the gas cooler. The heated water leaving the gas cooler then goes through the evaporator, recycling the heat collected from the gas cooler to re-evaporate the CO_2. A bypass line with a flow adjusting valve allows the superheat leaving the evaporator to be adjusted. The water leaving the evaporator and the bypass then goes to the drain connection. The CO_2 compressor was installed in a weather tight enclosure outside the building (Figure 5-7) with connecting CO_2 lines to the test loop inside the building.

Figure 5-6: Cooling Water Supply, Flow Control, and Drain Plumbing Arrangement

Figure 5-7: CO_2 Gas Compressor Installation

The mechanical layout of the test set up provides for measurement of the expander speed and torque output, speed control, and absorbing the shaft power output of the expander. The scroll expander and torque transducer are in line with each other, with a poly-vee belt drive pulley on the torque transducer. The electronic readout of the torque transducer measures both the torque and the speed accurately, providing a direct and accurate measurement of the shaft power output of the expander. An inverter driven, 5-horsepower motor sets the operating speed and a permanent magnet DC generator with load resistors on the output dissipates the shaft power produced by the expander. Figure 5-8 is a photograph of the motor and generator laid out in their position on the mounting plate, with the scroll expander mounting bracket and torque transducer placed next to the drive motor. Poly-vee belt drives transmit shaft power among these components.

To mount these components on the main base plate, mounting brackets were needed for the expander and the torque transducer and a mounting plate for the 5 horsepower motor was needed to provide a means of adjusting the belt tension. Pulleys for the poly-vee belt drive were fabricated, including a double-pulley for the 5 horsepower motor. A photograph these parts is shown in Figure 5-9

Figure 5-8: Motor and Generator Placed on Mounting Plate

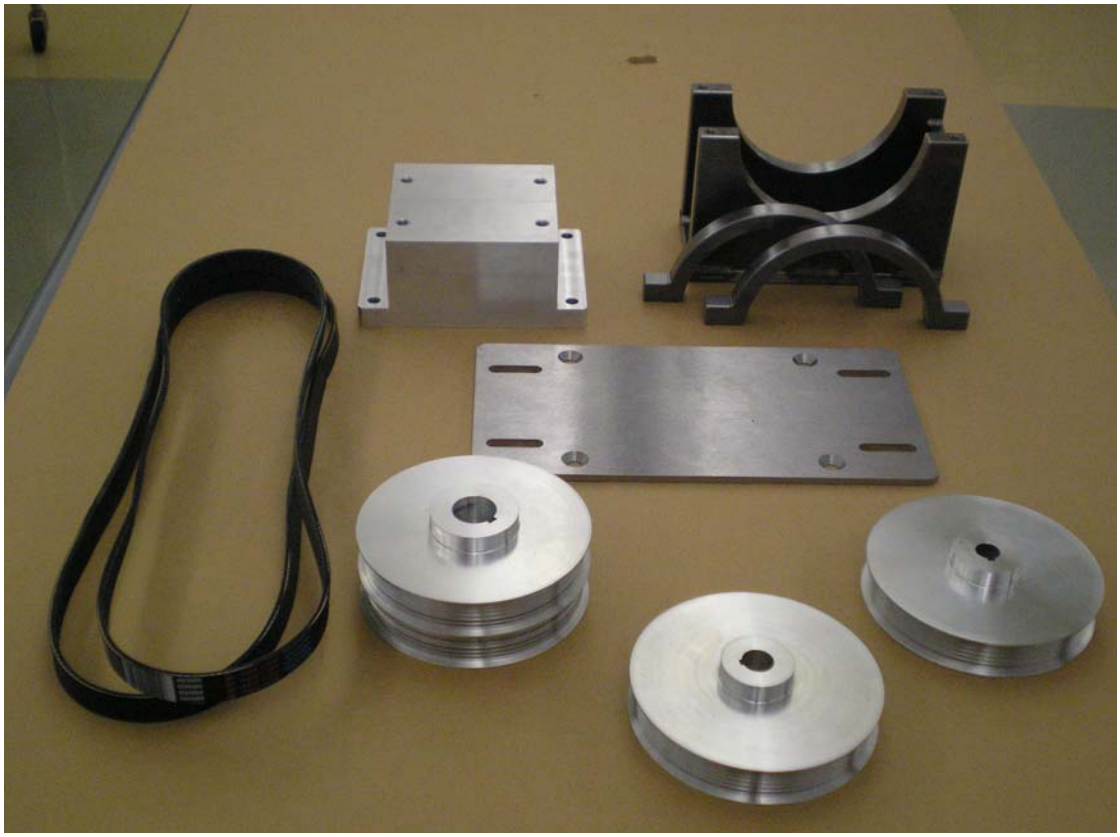

Figure 5-9: Mechanical Mounting Hardware

The oil separator, small diameter oil piping lines, pressure control lines, lines to pressure gauges, pressure relief valves, and evacuation and CO_2 charging ports were added to the components pictured above. The expander was connected to the CO_2 piping. Instrumentation – thermocouples, pressure gauges, pressure transducers, and water flow meters – was installed and the data acquisition system was set up. Figure 5-10 shows the overall test loop, with the completed CO_2 piping and cooling/heating water plumbing, the mechanical components and drive, and instrumentation, with the CO_2 expander installed.

Figure 5-10: Completed Test Loop

Figure 5-11 shows the expander as installed in the test loop. Major features are the CO_2 inlet from the high pressure side of the loop and the CO_2 outlet to the low side of the loop, an oil level sight glass, an oil level sensor, the oil feed line, the oil separator, and the housing pressure regulator. Mechanical features shown include the torque transducer connected to the output shaft of the expander with a helical coupling, the motor and the DC generator. The torque transducer measures the output torque generated by the expander and also measures the speed, providing a direct measurement of the mechanical power output of the expander. The motor is driven by a variable frequency drive and is used to set the speed for a given test condition. The permanent magnet DC generator absorbs the power produced by the expander.

Figure 5-12 shows the data acquisition system.

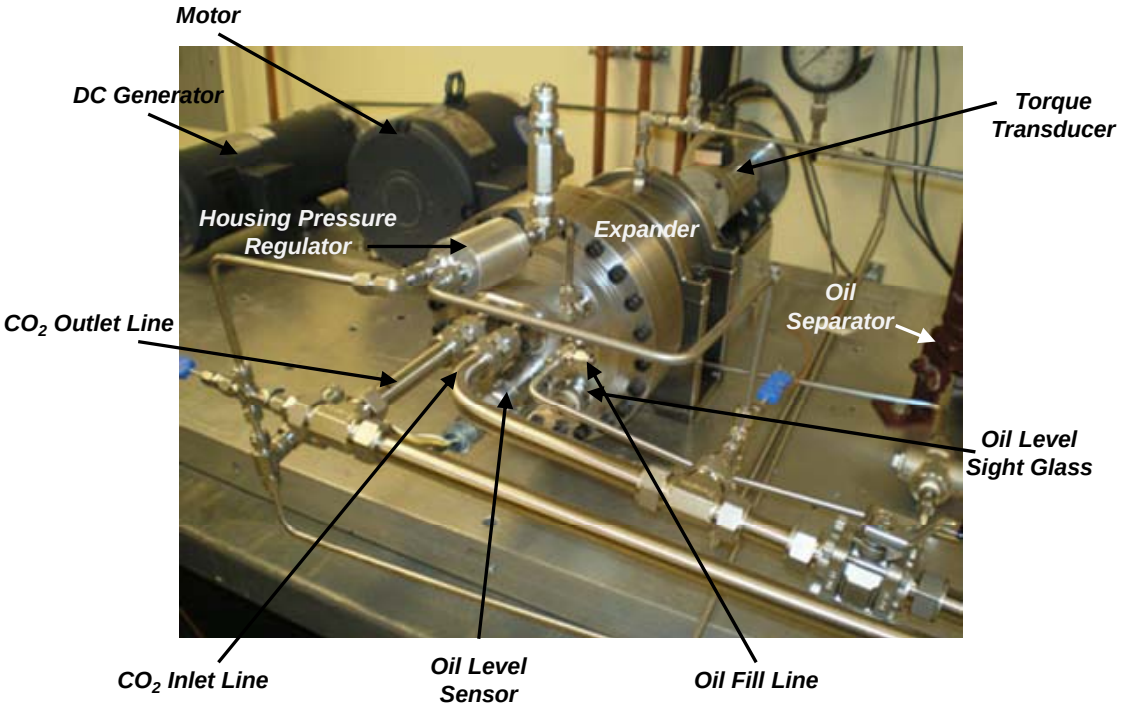

Figure 5-11: Expander as Installed in the Test Loop Showing the Mechanical Drive System to Absorb and Dissipate the Power Output of the Expander

Figure 5-12: Data Acquisition System

The heater load bank to absorb and dissipate power from the generator was designed, assembled, and checked out. The expander produces several horsepower of shaft power output. The mechanical system to dissipate this power and control the expander rotational speed consists of the expander output shaft, which is directly coupled to a torque transducer which in turn is coupled via a poly-vee belt drive to the pulley on a 5 horsepower, inverter driven electric motor, which in turn is coupled via belt drive to a brush-type permanent magnet DC motor, which is operated as DC generator, all shown in Figure 5-11. The torque transducer measures the output torque generated by the expander and also measures the speed, providing a direct measurement of the mechanical power output of the expander. The motor is driven by a variable frequency drive and is used to set the speed for a given test condition. The permanent magnet DC generator absorbs the power produced by the expander. The DC electric power output of the generator must be dissipated. The heater load bank consists of four finned strip electric resistance heaters of different wattage ratings and electric resistances. The four heaters are connected in parallel through individual on-off switches. As the speed varies, the output voltage of the DC generator varies. An appropriate combination of these heaters can be selected to draw the rated full load current output of the DC generator. The heater load bank is packaged in a metal enclosure and is fan cooled. Figure 5-13 shows the load bank.

The torque transducer was calibrated using a lever arm and weights. The lever arm was clamped to the coupling between the expander and the torque transducer. The other end of the torque transducer shaft was restrained with a wrench. As various weights were placed on the lever arm at a 9 inch radius, the resulting torque and millivolt output of the torque transducer into the data acquisition system was noted and a calibration curve was developed.

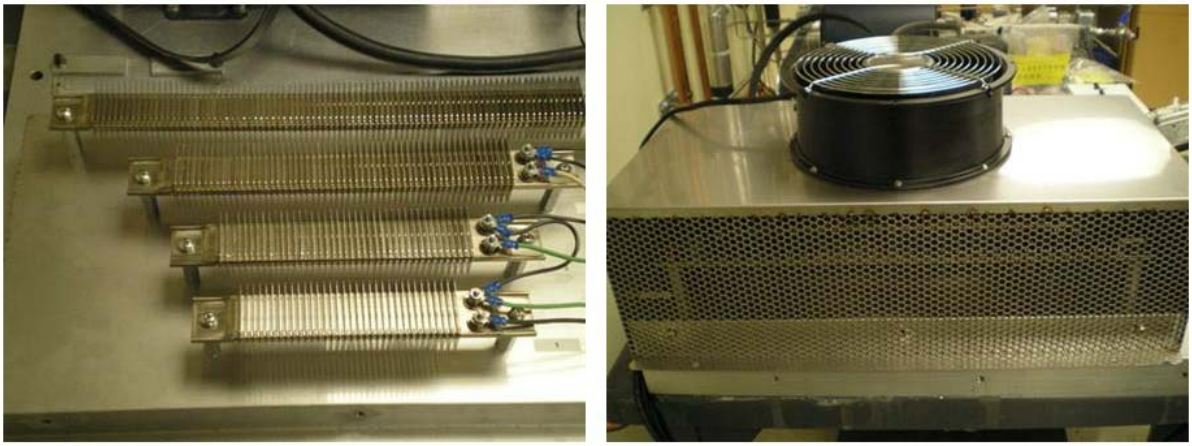

Figure 5-13; Heater Load Bank – Finned Strip Heaters on the Left, the Complete Enclosure with Cooling Fan on the Right

5.2 Test Results

5.2.1 Development Testing

First the CO_2 compressor was started up. The CO_2 compressor is a Dorin model TCS362-D, single cylinder semi-hermetic compressor which is driven by a variable frequency drive (VFD). The input voltage to the inverter and to the compressor at maximum speed (3500 RPM at 60 Hz)

is 460 VAC, 60 Hz, 3 phase, the compressor is approved by the manufacturer to run on inverter power, over an input frequency range of 25 Hz to 60 Hz. The compressor was operated over the rated frequency range and a range of output pressures, with the expander bypassed. The compressor operated smoothly, with electric current draw within the expected range and rated capacity of the VFD. With the expander bypassed, the CO_2 loop was operating as a CO_2 refrigeration system with a throttled expansion and producing a significant amount of cooling. One issue that was noticed and partially corrected was the transmission of a significant amount of noise from the outdoor location of the compressor into the building via the connecting piping. By replacing some rigid mountings of the pipe with flexible mounts the noise was reduced considerably. We added several other noise attenuating features – flexible pipe loops on the discharge and inlet lines near the compressor and inlet and discharge mufflers.

Next we began running the expander, at inlet pressures between 1200 psig and 1300 psig, outlet pressures between 600 psig and 650 psig, and speeds of 900, 1200, 1350, 1500, 1650, and 1800 RPM (1800 RPM is the design speed). Table 5-1 summarizes the test data at 1200, 1500, and 1800 RPM. The basic performance metric is that the isentropic efficiency varied from 53.6% at 1200 RPM to 58.0% at 1500 RPM to 62.9% at 1800 RPM. The goal of the project is 75% isentropic efficiency at the 1800 RPM design speed. The last three line items of Table 5-1 are the ideal CO_2 mass flow rate (based on the inlet displacement, RPM, and CO_2 inlet density), the CO_2 leakage mass flow rate (internal leakage through the scrolls, the difference between the actual and ideal mass flow rate), and the ratio of actual to ideal CO_2 mass flow rate though the expander. We expected the CO_2 leakage mass flow though the scrolls to typically be about 10% of the ideal mass flow rate, the levels measured in this initial test were quite a bit higher. We expected that small errors in the scroll geometry are the likely reason for the excess mass flow. To diagnose this, we sent the scroll parts to an outside machine shop with an accurate coordinate measuring machine (Zeiss Calypso). The output torque was much closer to ideal levels, indicating that the expander has a high mechanical efficiency.

Table 5-1: Summary of First Set of Expander Test Data

Expander, Speed, RPM	1200	1500	1800
Inlet Pressure, psia	1245	1220	1205
Outlet Pressure, psia	633	635	655
Inlet Temperature, °F	99.7	99.1	98.2
Expander output Torque, in-lbf	87	82	70
Shaft Power, Horsepower	1.66	1.95	2.00
CO_2 Mass Flow Rate, lb/hr	1502	1560	1562
Isentropic Power, Horsepower	3.09	3.37	3.18
Isentropic Efficiency	53.6%	58.0%	62.9%
Ideal (no internal leakage) Mass Flow Rate, lb/hr	878	994	1165
Internal Leakage Flow Rate, lb/hr	624	566	397
Actual Mass Flow/Ideal Mass Flow	1.71	1.57	1.34

After these test runs, the expander was disassembled to inspect the moving parts as well as to get the scroll parts out to send them out for dimension inspection. Bearing surfaces of the orbital drive mechanism were in very good condition indicating that hydrodynamic lubrication was

being obtained at all of these bearing surfaces, consistent with the observed high mechanical efficiency. Scroll flank surfaces showed no signs of wear, the thrust bearing surface was similarly in good shape. In the center bulb area of the fixed scroll and the mating base surface of the orbiting scroll, some wear was observed, which we think occurred when the orbital drive pressure was too high, squeezing the scrolls together too hard.

One thing we had noticed while calculating the isentropic efficiency for development test runs completed in the previous quarter is that at some combinations of expander inlet temperature and pressure, for example 100°F and 1,200 psig, the calculated efficiency is very sensitive to the exact temperature and pressure. The complete test matrix of expander inlet temperatures and pressures includes several points where there is less sensitivity to precise pressure and temperature measurement, for example at 110°F and 1,500 psig and at 110°F and 1,800 psig. However the entire matrix corresponds to real-world conditions, so accurate measurement of the efficiency is needed across the entire matrix. Accordingly, we upgraded the expander inlet pressure and temperature measurements. We purchased a 0 to 2,000 psi Heise gauge to measure inlet pressure and have purchased a platinum RTD with a supporting electronics module to measure the inlet temperature. The calibration of the RTD and electronics module was checked in an ice bath and found to be accurate within 0.05°F.

The inspection results, summarized in Table 2, indicated that the scroll parts were out of tolerance by a small amount, not enough to account for the leakage mass flow rate mentioned above. Further examination of the design and parts turned up two important design and fabrication issues that needed to be corrected.

Table 5-2: Inspection Data for First Set of Prototype Scrolls

Scroll & Curve	*Nominal Radius (inch)*	*Max Actual R – Nominal (inch)*	*Minimum Actual R-Nominal (inch)*
Fixed, Inner Wall	0.578	+0.0004	-0.0008
	0.908	+0.0013	0
	1.238	+0.0004	-0.0009
	1.568	+0.0013	-0.0004
	1.898	-0.0006	-0.0009
Fixed, Outer Wall	0.413	+0.0007	-0.0005
	0.743	+0.0001	-0.0013
	1.073	+0.0007	-0.0006
	1.403	-0.0005	-0.0013
Orbiting, Inner Wall	0.248	+0.0002	-0.0002
	0.578	+0.0005	-0.0005
	0.908	+0.0004	-0.0005
	1.238	+0.0005	-0.0002
	1.568	-0.0005	-0.0007
Orbiting, Outer Wall	0.413	+0.0004	-0.0004
	0.743	+0.0004	-0.0003
	1.073	0	-0.0006
	1.403	+0.0003	-0.0005
	1.733	-0.0003	-0.0006

First, the scroll form was generated as a series of 180 degree arcs. The arcs are used because CNC milling machines have excellent arc generation software. When revisiting the gas pressure forces, we noticed an unanticipated consequence of the high CO_2 pressures and the 180 arcs. The gas pressure force component that acts to push the orbiting scroll radially inward (i.e., to separate it from contacting the fixed scroll) is normally small in relationship to the centrifugal force pushing the orbiting scroll into contact with the fixed scroll, but with the high CO_2 pressures, the gas pressure and centrifugal forces are comparable. The 180 degree arc generation results in the radial gas pressure force cycling twice per full orbit from zero to a maximum that is greater than the centrifugal force. This tends to cause the scrolls to be driven apart (opening up a leakage path), then slamming back together (generating mechanical noise), as the gas pressure force cycles from zero to maximum and back. The only remedy for this is to modify the scroll form to more closely approximate a pure involute spiral (involute of a circle). We opted to do this using a series of 90 degree arcs, much more closely approximating involute spirals, while retaining the advantage of using the arc generation software embedded in CNC machines. To implement this, it was necessary to modify the design and machine and inspect a new set of scrolls. The new set of scrolls has been inspected and found to be very close to the tight tolerances, the inspection data is summarized in Table 5-3.

Second, we evaluated the free travel of the Oldham coupling keys in the Oldham coupling slots and found that the free travel was somewhat less than the two orbit radiuses of free travel that are needed. This interferes to a degree with the scroll orbiting at the full orbit radius and could easily account for the observed internal leakage flow discussed above. The slots were remachined to provide the necessary two orbit radiuses of free travel plus an extra 0.060 inch to ensure that no jamming occurs at the extremes of Oldham coupling motion.

The new scrolls were assembled into the expander, along with the other reworked parts (as described in the previous paragraphs). An initial test was run with the new configuration. The CO_2 mass flow rate was high relative to the inlet displacement-speed- inlet density product indicating high internal leakage, while the output torque was close to ideal levels, indicating that the expander is operating with a high mechanical efficiency. Modifications were made to the test loop to enable improved diagnosis of CO_2 mass flow. Modifications were also made to improve oil management in both the expander and in the overall CO_2 test loop. Further testing was put on hold, pending receipt of the aforementioned Heise pressure gauge.

Table 5-3: Inspection Data for Second Set of Prototype Scrolls

CMM Radii Measurements on Fixed Scroll D0566-0065						
	Nominal Radius	Average Measured Radius	Max Reading - Nominal	Min Reading - Nominal	Average Reading - Nominal	Standard Deviation: Radius
Curve Form Outer	1.8975	1.8977	0.0004	-0.0005	-0.0002	0.0002
	1.7325	1.7324	0.0001	-0.0006	0.0001	0.0001
	1.5675	1.5674	0.0001	-0.0003	0.0001	0.0001
	1.4025	1.4029	0.0006	0.0001	-0.0004	0.0001
	1.2375	1.2378	0.0004	-0.0001	-0.0003	0.0001
	1.0725	1.0724	0.0001	-0.0003	0.0001	0.0001
	0.9075	0.9074	0.0003	-0.0003	0.0001	0.0001
	0.7425	0.7429	0.0006	0.0002	-0.0004	0.0001
Curve Form Inner	1.4025	1.4024	0.0001	-0.0003	0.0001	0.0001
	1.2375	1.2371	-0.0002	-0.0006	0.0004	0.0001
	1.0725	1.0721	-0.0002	-0.0005	0.0004	0.0001
	0.9075	0.9076	0.0008	-0.0002	-0.0001	0.0002
	0.7425	0.7425	0.0002	-0.0003	0.0000	0.0002
	0.5775	0.5770	-0.0003	-0.0006	0.0005	0.0001
	0.4125	0.4122	-0.0001	-0.0006	0.0003	0.0001
	0.2475	0.2475	0.0001	-0.0002	0.0000	0.0001
CMM Radii Measurements on Orbital Scroll D0566-0066						
	Nominal Radius	Average Measured Radius	Max Reading - Nominal	Min Reading - Nominal	Average Reading - Nominal	Standard Deviation: Radius
Curve Form Outer	1.7325	1.7317	-0.0005	-0.0010	0.0008	0.0001
	1.5675	1.5673	0.0000	-0.0007	0.0002	0.0002
	1.4025	1.4025	0.0002	-0.0002	0.0000	0.0001
	1.2375	1.2370	-0.0001	-0.0008	0.0005	0.0002
	1.0725	1.0717	-0.0006	-0.0009	0.0008	0.0001
	0.9075	0.9073	0.0001	-0.0006	0.0002	0.0002
	0.7425	0.7425	0.0003	-0.0003	0.0000	0.0001
	0.5775	0.5771	-0.0001	-0.0007	0.0004	0.0002
Curve Form Inner	1.5675	1.5673	0.0000	-0.0005	0.0002	0.0001
	1.4025	1.4028	0.0006	-0.0008	-0.0003	0.0003
	1.2375	1.2381	0.0007	0.0005	-0.0006	0.0001
	1.0725	1.0726	0.0004	-0.0002	-0.0001	0.0002
	0.9075	0.9073	0.0000	-0.0003	0.0002	0.0001
	0.7425	0.7428	0.0006	0.0000	-0.0003	0.0002
	0.5775	0.5781	0.0007	0.0004	-0.0006	0.0001
	0.4125	0.4125	0.0003	-0.0008	0.0000	0.0004

Testing was resumed after the Heise pressure gauge was installed. While the oil management improvements facilitated testing, we found two additional shortcomings that needed to be remedied. First, in the configuration where the expander is being tested by itself, there has been a gradual transfer of oil from the expander sump to the compressor sump, in excess of the rate that oil is carried over from the compressor to the oil separator, where it can be supplied to the expander sump. As a result, excess oil needed to be removed from the compressor sump and

replenished to the expander, severely limiting run time. Second, we have observed that at a given set of conditions (inlet and out pressures), the performance was highly sensitive to the intermediate pressure level in the orbital drive mechanism, which seemed to be due to the limited load capacity of the purely hydrodynamic thrust bearing. To address these issues, further modifications were carried out, adding an oil feed reservoir and an auxiliary oil sump to the expander and adding a pressurized oil feed to the thrust bearing, to increase the capacity of the thrust bearing, so a wider range of intermediate pressures could be used at any condition. With these modifications, a set of tests were run. At 1,800 RPM, performance close the original performance goal of the project was achieved, as summarized in the following three data sets. At each of these points the isentropic efficiency was over 70% (75% is the goal for the project), with a maximum of 76.4

Carbon Dioxide Scroll Expander Test

Inputs - Enter data to cells with stored values

State	*Temperature*		*Pressure*		*Volumetric Flow*	
CO_2 Gas Cooler In	102.8	°C	1215	psia		
CO_2 Gas Cooler Out	38.9	°C	1213	psia		
H_2O Gas Cooler In	35	°C	14.7	psia	4.7	gpm
H_2O Gas Cooler Out	51.5	°C	14.7	psia	3.45	gpm
CO_2 Expander Out	2.6	°C	549.7	psia		
CO_2 Evaporator Out	23.8	°C	539.7	psia		
H_2O Evaporator Out	34.3	°C	14.7	psia		
Expander Output Torque	90.8	in-lb				
Expander Output RPM	1800	rpm				
Intermediate Pressure	889.7	psia				

Control Cells	
Units	C
Fluids	CO2
	Water

Outputs

State	*Enthalpy*		*Entropy*		*Density*		*Mass Flow*		*Quality*	
H_2O Gas Cooler In	146.7	kJ/kg	0.505	kJ/kg-K	994.0	kg/m^3	0.295	kg/s		
H_2O Gas Cooler Out	215.7	kJ/kg	0.723	kJ/kg-K	987.3	kg/m^3	0.295	kg/s		
CO_2 Gas Cooler In	520.8	kJ/kg	2.001	kJ/kg-K	147.3	kg/m^3	0.141	kg/s		
CO_2 Gas Cooler Out	377.0	kJ/kg	1.571	kJ/kg-K	353.6	kg/m^3	0.141	kg/s		
Ideal CO_2 Expander Out	358.2	kJ/kg	1.571	kJ/kg-K	1181.5	kg/m^3	0.119	kg/s	68.01	%
CO_2 Expander Out	363.3	kJ/kg	1.590	kJ/kg-K	146.4	kg/m^3	0.141	kg/s	70.35	%
CO_2 Evaporator Out	462.9	kJ/kg	1.949	kJ/kg-K	85.3	kg/m^3	0.141	kg/s		
H_2O Evaporator Out	143.8	kJ/kg	0.496	kJ/kg-K	994.3	kg/m^3	0.215	kg/s		
Expander Work	1.93	kW								
Ideal Expander Work	2.67	kW								
Expander Isentropic Eff	72.55	%								
Heat Leak Rate (Evap)	-1.38	kW								
Actual/Ideal Mass Flow	1.19									

Carbon Dioxide Scroll Expander Test

Inputs - Enter data to cells with stored values							
State	*Temperature*		*Pressure*		*Volumetric Flow*		
CO_2 Gas Cooler In	105.8	°C	1240	psia			
CO_2 Gas Cooler Out	39.6	°C	1235	psia			
H_2O Gas Cooler In	35	°C	14.7	psia	4.7	gpm	
H_2O Gas Cooler Out	51.7	°C	14.7	psia	3.45	gpm	
CO_2 Expander Out	2.7	°C	554.7	psia			
CO_2 Evaporator Out	25.2	°C	544.7	psia			
H_2O Evaporator Out	34.5	°C	14.7	psia			
Expander Output Torque	91.9	in-lb					
Expander Output RPM	1800	rpm					
Intermediate Pressure	924.7	psia					

Control Cells	
Units	C
Fluids	CO2
	Water

Outputs										
State	*Enthalpy*		*Entropy*		*Density*		*Mass Flow*		*Quality*	
H_2O Gas Cooler In	146.7	kJ/kg	0.505	kJ/kg-K	994.0	kg/m^3	0.295	kg/s		
H_2O Gas Cooler Out	216.5	kJ/kg	0.726	kJ/kg-K	987.3	kg/m^3	0.295	kg/s		
CO_2 Gas Cooler In	523.6	kJ/kg	2.005	kJ/kg-K	148.6	kg/m^3	0.137	kg/s		
CO_2 Gas Cooler Out	373.8	kJ/kg	1.560	kJ/kg-K	367.9	kg/m^3	0.137	kg/s		
Ideal CO_2 Expander Out	355.2	kJ/kg	1.560	kJ/kg-K	1186.9	kg/m^3	0.124	kg/s	66.61	%
CO_2 Expander Out	359.6	kJ/kg	1.576	kJ/kg-K	151.1	kg/m^3	0.137	kg/s	68.61	%
CO_2 Evaporator Out	464.2	kJ/kg	1.952	kJ/kg-K	85.5	kg/m^3	0.137	kg/s		
H_2O Evaporator Out	144.6	kJ/kg	0.498	kJ/kg-K	994.2	kg/m^3	0.215	kg/s		
Expander Work	1.96	kW								
Ideal Expander Work	2.56	kW								
Expander Isentropic Eff	76.43	%								
Heat Leak Rate (Evap)	-1.07	kW								
Actual/Ideal Mass Flow	1.11									

Carbon Dioxide Scroll Expander Test

Inputs - Enter data to cells with stored values						
State	*Temperature*		*Pressure*		*Volumetric Flow*	
CO_2 Gas Cooler In	106.3	°C	1235	psia		
CO_2 Gas Cooler Out	40	°C	1232	psia		
H_2O Gas Cooler In	34.9	°C	14.7	psia	4.6	gpm
H_2O Gas Cooler Out	52.4	°C	14.7	psia	3.45	gpm
CO_2 Expander Out	3.9	°C	569.7	psia		
CO_2 Evaporator Out	26	°C	554.7	psia		
H_2O Evaporator Out	34.8	°C	14.7	psia		
Expander Output Torque	91.6	in-lb				
Expander Output RPM	1800	rpm				
Intermediate Pressure	919.7	psia				

Control Cells	
Units	C
Fluids	CO2
	Water

Outputs										
State	*Enthalpy*		*Entropy*		*Density*		*Mass Flow*		*Quality*	
H_2O Gas Cooler In	146.3	kJ/kg	0.504	kJ/kg-K	994.1	kg/m^3	0.288	kg/s		
H_2O Gas Cooler Out	219.5	kJ/kg	0.735	kJ/kg-K	986.9	kg/m^3	0.288	kg/s		
CO_2 Gas Cooler In	524.5	kJ/kg	2.008	kJ/kg-K	147.5	kg/m^3	0.145	kg/s		
CO_2 Gas Cooler Out	379.0	kJ/kg	1.577	kJ/kg-K	352.3	kg/m^3	0.145	kg/s		
Ideal CO_2 Expander Out	360.5	kJ/kg	1.577	kJ/kg-K	1189.0	kg/m^3	0.119	kg/s	68.90	%
CO_2 Expander Out	365.6	kJ/kg	1.595	kJ/kg-K	151.1	kg/m^3	0.145	kg/s	71.24	%
CO_2 Evaporator Out	464.3	kJ/kg	1.949	kJ/kg-K	87.1	kg/m^3	0.145	kg/s		
H_2O Evaporator Out	145.9	kJ/kg	0.502	kJ/kg-K	994.1	kg/m^3	0.215	kg/s		
Expander Work	1.95	kW								
Ideal Expander Work	2.69	kW								
Expander Isentropic Eff	72.64	%								
Heat Leak Rate (Evap)	-1.49	kW								
Actual/Ideal Mass Flow	1.22									

Testing was continued, first replacing the rectangular cross section Teflon seal ring between the thrust bearing oil film and the scroll area with a Vee ring seal. The Vee seal did not perform as well as the original Teflon seal, resulting in less effective thrust bearing performance, as evidenced by reduced thrust bearing oil film pressure, even with increased oil flow. A set of tests were run with isentropic efficiencies of approximately 60%, with inlet pressures ranging from 1200 psia to 1500 psia.

A new rectangular cross section oil seal was installed and testing was repeated. Again the thrust bearing seal performance was subpar and similar results were obtained.

The contrast between the previously reported result and the more recent results highlights the importance of robust thrust bearing performance to the overall performance of the expander. We pursued measures to improve the seal performance and if necessary to increase the oil feed flow

rate to the bearing. Two more thrust bearing oils seals were fabricated, from glass-filled Teflon. Performance was tested with one of these seals and with increased oil feed rate to the thrust bearing. Isentropic efficiencies in the mid 60% range were obtained, better that recent tests, but not as good as the results reported in July. To move the isentropic efficiency up into the mid 70% range, an improved oil seal, enabling the oil film pressure to exceed the intermediate pressure will be necessary. In the current program, we opted to move ahead to the expander performance test and compressor testing tasks.

5.2.2 Expander Performance Testing

A set of performance tests were run, the results at several data points are summarized in Table 5-4.

Table 5-4: Expander Performance Test Data

RPM	Inlet Pressure psia	Outlet Pressure psia	Isentropic Efficiency %
1,200	1,200	600	55.0
1,500	1,200	600	64.7
1,800	1,200	600	62.7
1,200	1,500	650	54.1
1,500	1,500	650	61.6
1,800	1,500	650	64.9

In these tests the oil film pressure was consistently below the intermediate pressure, limiting our ability to force close tip clearance operation with low friction loss in the thrust bearing, as described above. Again, for the time being, we opted to move on to the compressor testing task.

6.0 Compressor Design

6.1 Design

The integrated scroll compressor and scroll expander combined the existing expander with an appropriately sized scroll compressor. To provide a hermetic motor that is compatible with CO_2 and suitable lubricants, we purchased a Bock semihermetic CO_2 compressor. The housing of this compressor, with the electric motor, was used as a platform for mounting the scroll compressor and expander assemblies. The compressor housing and the common drive shaft were designed to interface with the Bock Compressor housing.

6.2 Supporting Analysis

Finite element analysis of the stresses and deflections resulting from the anticipated pressure loading on the scroll parts was completed. The primary concern is with the axial deflection of the scroll disc under the pressure loading, impacting the axial clearances. Based on the FEA results, the thickness of the two scroll discs was adjusted so the maximum expected deflection is no more than 0.0002 inches. Figures 6-1 through 6-4 show the results of the FEA at the final disc thicknesses.

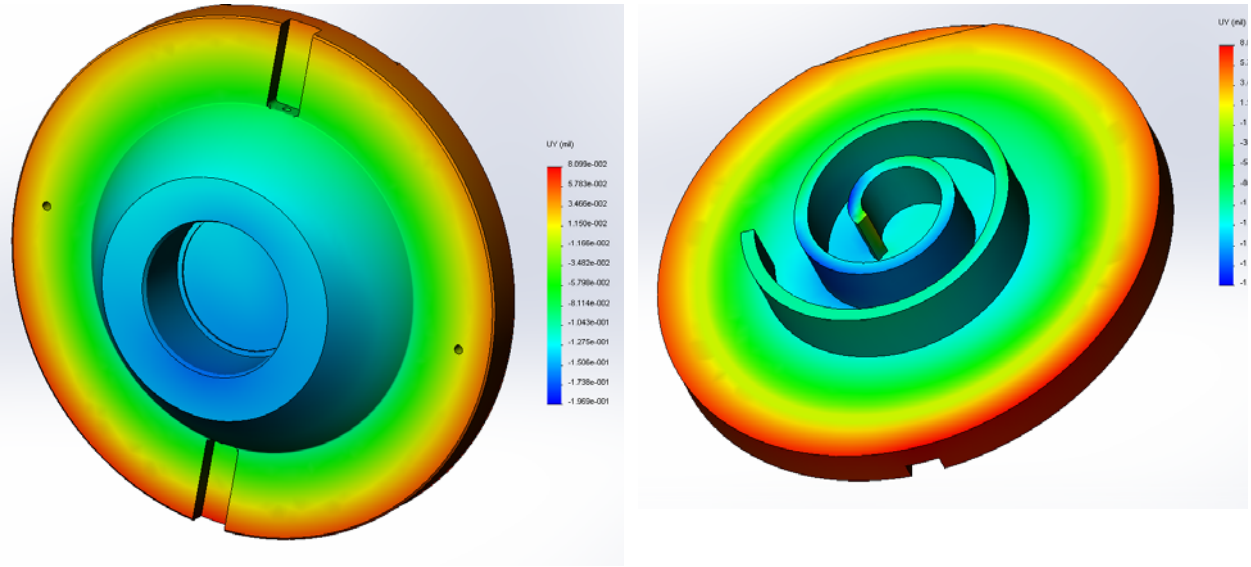

Figure 6-1: Orbiting Scroll FEA Axial Deflection Results at 0° Orbital Position

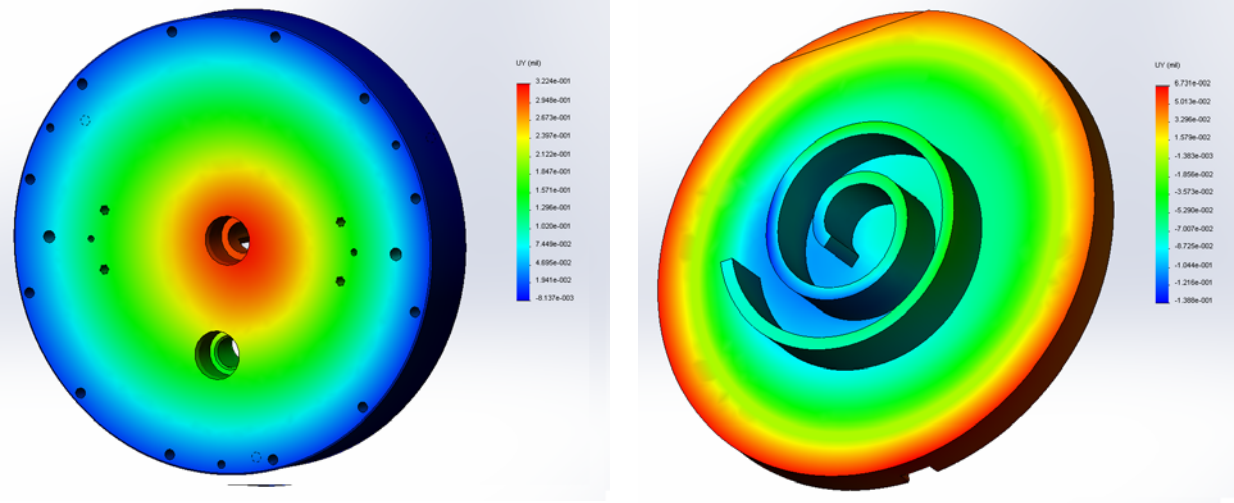

Figure 6-2:Orbiting Scroll FEA Axial Deflection Results at 180^{o} Orbital Position

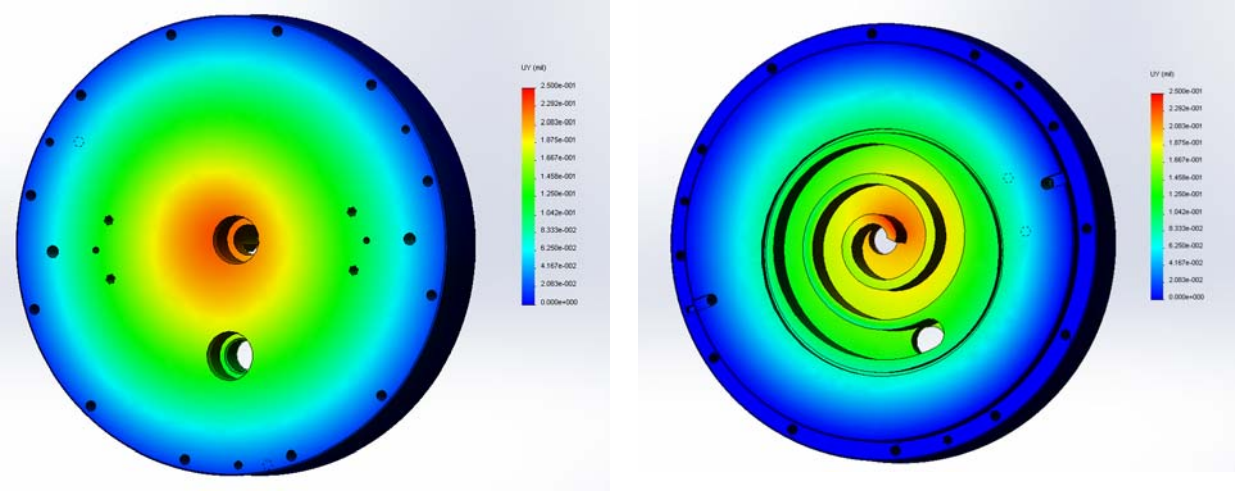

Figure 6-3: Fixed Scroll FEA Axial Deflection Results at 0^{o} Orbital Position

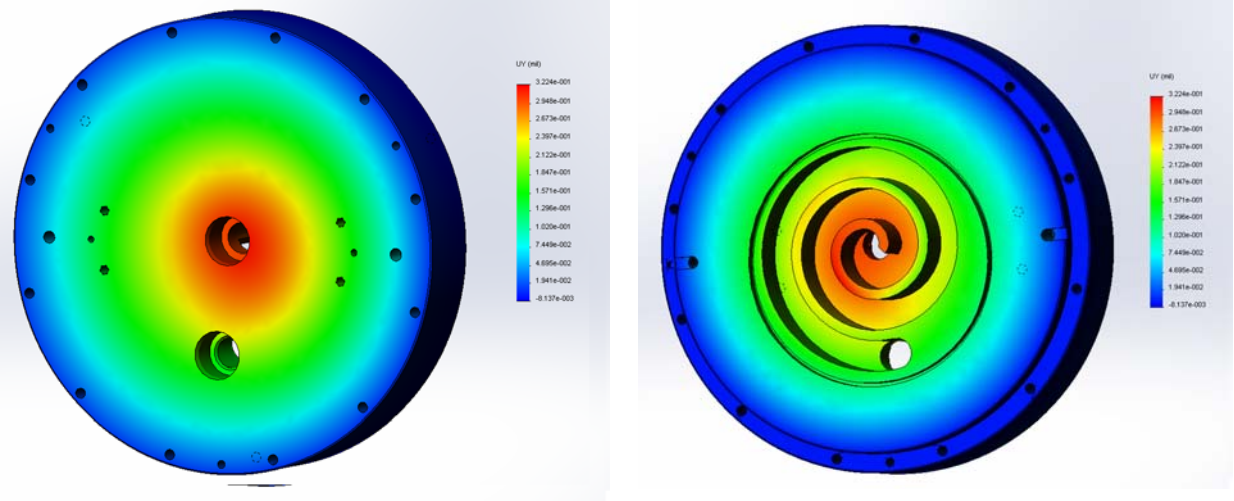

Figure 6-4: Fixed Scroll FEA Axial Deflection Results at 180^{o} Orbital Position

Figure 6-5 is a schematic of the lubrication and oil management system. It has been designed to accomplish several objectives:

- Feed oil under pressure to two scroll thrust bearings and two shaft bearings
- Feed oil to the compressor inlet to ensure scroll lubrication and to enhance sealing between the two scrolls
- Maintain oil levels in the compressor and expander orbital drive units to provide splash lubrication for the Oldham couplings and orbiting scroll drive bearings
- Provide motor cooling

From Figure 6-5, oil entrained in the compressor discharge CO_2 flow is separated from this flow and drained into a reservoir. The CO_2, with minimal entrained oil continues on to the gas cooler, the expander, and the evaporator, returning to the compressor inlet. The separated oil, at high-side pressure, is supplied to the four bearings – two scroll thrust bearings and two main shaft bearings. This oil passes through these four bearings and drains into the compressor or the expander orbital drive units. As oil flows into the orbital drive units, the oil level rises to overflow tubes located at the correct orbital drive oil level. Overflowing oil drains to an intermediate pressure oil reservoir. Oil from this reservoir is metered by a capillary tube to the compressor inlet. Another loop from the intermediate pressure oil reservoir circulates oil through an oil cooler, then to the drive motor to cool the motor.

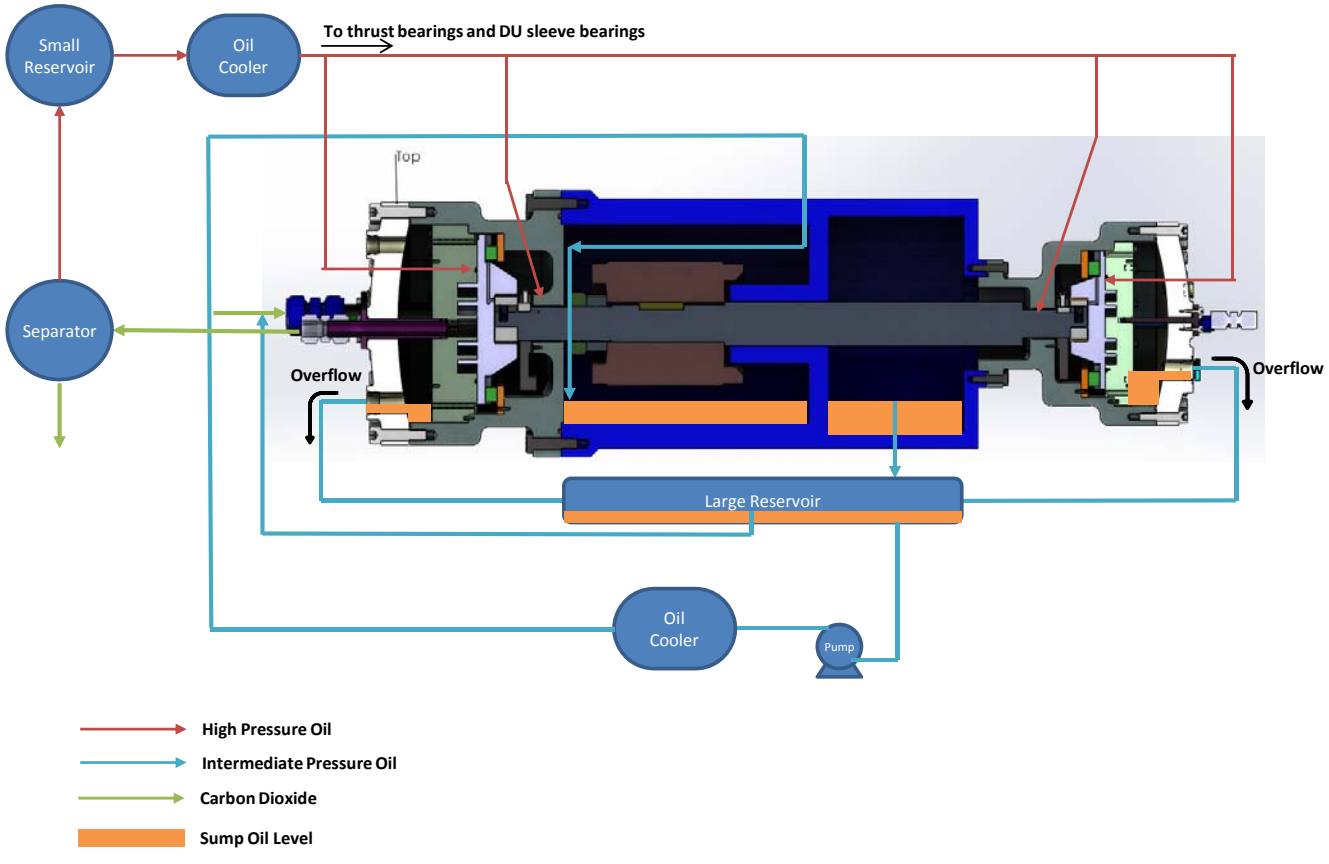

Figure 6-5: Lubrication and Oil Management System for the Compressor and for the Integrated Compressor and Expander

Table 6-1 summarizes the bearing performance calculations for the integrated compressor and expander. There are four hydrodynamically lubricated sleeve bearings – two that support the motor/drive shaft, and one drive bearing each for the compressor and expander orbiting scrolls. At design loads, estimated minimum oil film thicknesses are greater than 300 microinches for all four bearings. The total power loss in the four bearings is less than 1 horsepower.

Table 6-1: Bearing Calculations

INPUTS		*Exp Scroll Brg*	*Exp DU Brg*	*Comp DU Brg*	*Comp Scroll Brg*
Load	W, lb	982	1042	2484	2236
Shaft Speed	N, rpm	1750	1750	1750	1750
Journal Diameter	D, in	1.75	1.25	1.5	2
Bearing Bore	Db, in	1.752	1.252	1.502	2.002
Bearing Length	L, in	0.75	1	1.25	1
Lubricant Density	γ, lb/gal	8.33	8.33	8.33	8.33
Lubricant Viscosity	Z, cP	68	68	68	68
Lubricant specific heat	Cp, Btu/lbm-°F	0.482	0.482	0.482	0.482
Lubricant inlet temp	T1, °F	100	100	100	100
OUTPUTS					
Radial Clearance	C, in	0.001	0.001	0.001	0.001
Clearance Factor	m	1.14	1.60	1.33	1.00
Length to Dia Ratio	L/D	0.43	0.80	0.83	0.50
Bearing characteristic number	A	0.0035	0.0143	0.0165	0.0047
Eccentricity ratio	ε	0.7	0.64	0.63	0.64
Frictional power factor	kf	0.058	0.027	0.026	0.051
Frictional power loss	Pf, hp	0.20	0.10	0.23	0.40
Side leakage flow factor	kq	1.85	3	3	2
Lubricant feed rate	Q, gpm	0.020	0.016	0.024	0.028
Min feed rate	Q', gpm	0.0006	0.0006	0.0013	0.0012
Temp rise in bearing with Q	T2 - T1, °F	106	63	101	151
Outlet lubricant temperature	T2, °F	206	163	201	251
Minimum film thickness	mil	0.30	0.36	0.37	0.36

7.0 Compressor Fabrication

Fabrication of the compressor scroll parts was completed. Figure 7-1 shows photographs of the two scroll parts. Figure 7-2 is a photograph of the Bock compressor housing with the motor stator. Figure 7-3 is a photograph of the compressor housing for the integrated compressor and expander prototype. Figure 7-4 is a photograph of the expander housing for the integrated compressor and expander prototype. Figure 7-5 is a photograph of the moving parts of the compressor. Figure 7-6 is a photograph of the compressor and expander housings assembled with the Bock compressor housing.

Figure 7-1: Fixed and Orbiting Scroll Parts for the Compressor

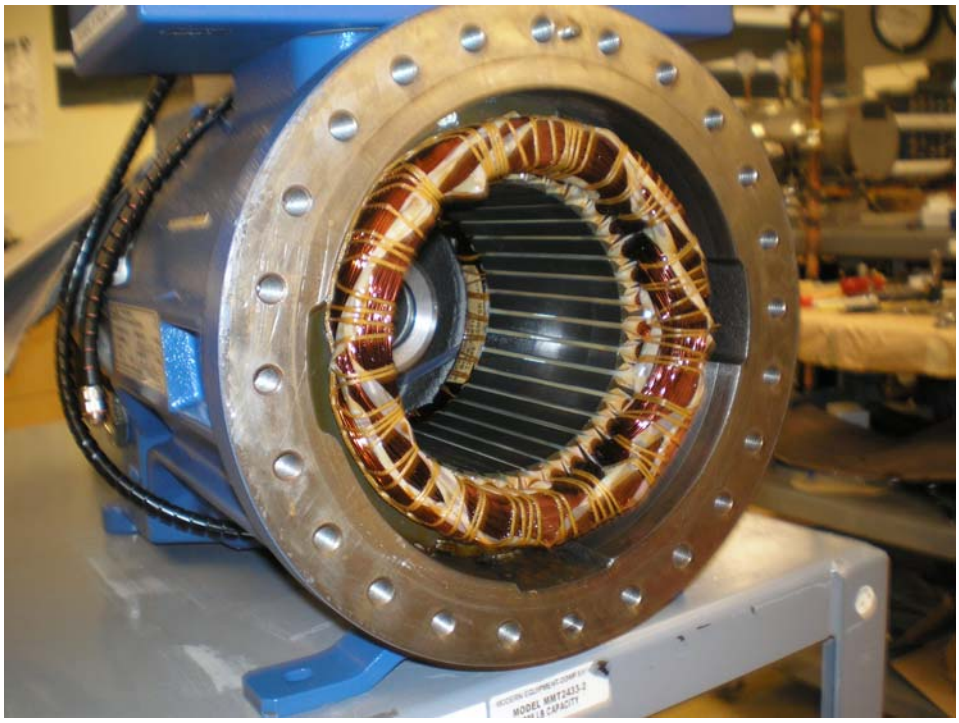

Figure 7-2: Bock Compressor Housing with Motor Stator

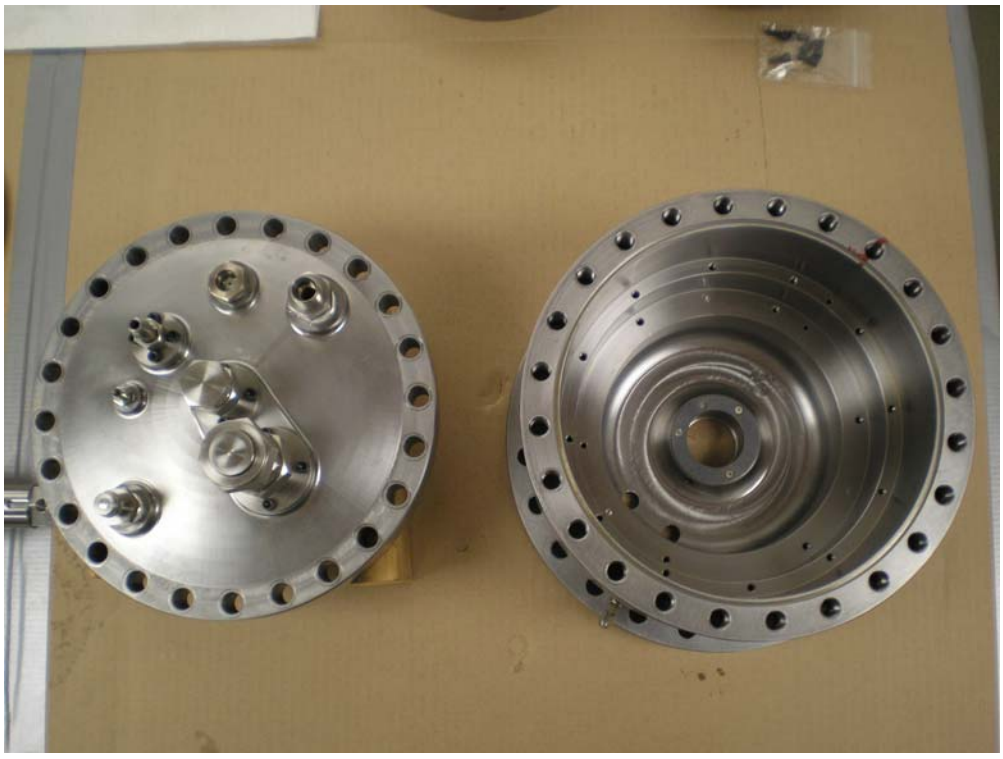

Figure 7-3: Compressor Housing and End Cover

Figure 7-4: Expander Housing

Figure 7-5: Compressor Moving Parts (Shaft, Motor Rotor, Oldham Coupling and Counterweight)

Figure 7-6: Compressor and Expander Housings Assembled with Bock Compressor Housing

8.0 Compressor Testing

8.1 Test Loop

Figure 8-1 is a flow schematic of the test loop, configured for testing the compressor. The same gas cooler and evaporator were used as were used for expander testing. The residual PAG oil in the gas cooler and evaporator were flushed out prior to connecting the compressor with POE oil. Not shown in Figure 8-1 are multiple pressure and temperature measurement points. Figures 8-2 and 8-3 are photographs of the compressor installed in the test loop.

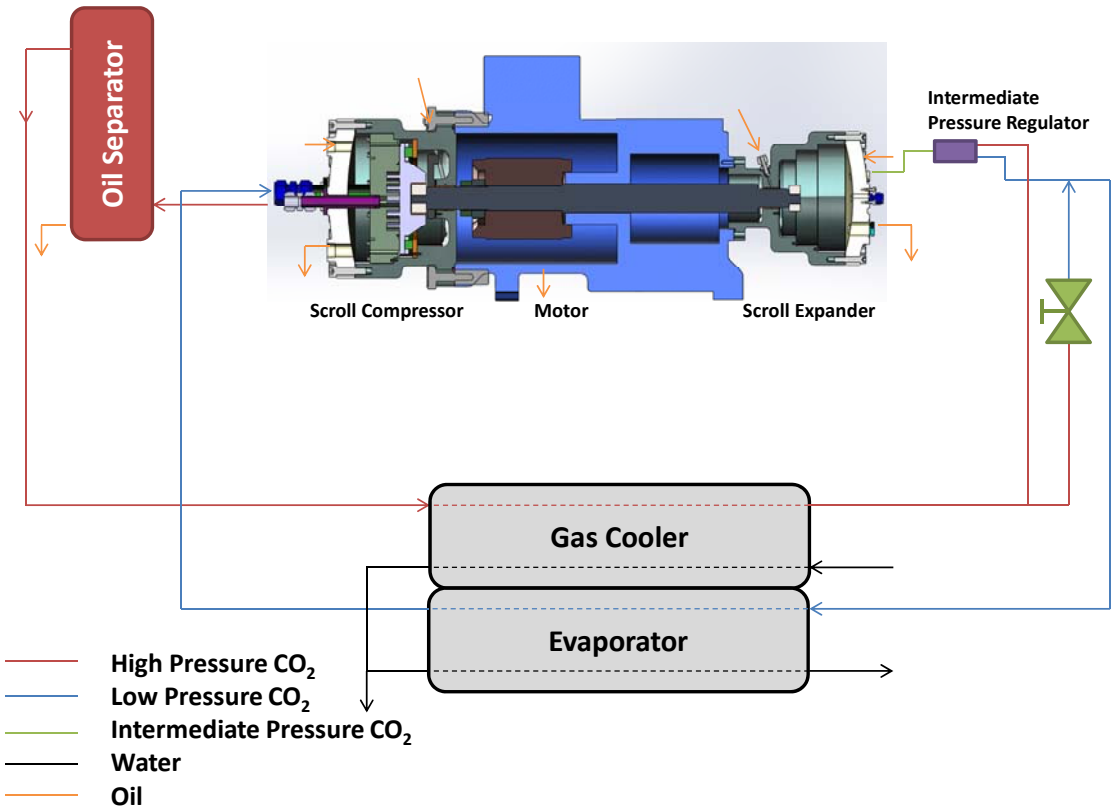

Figure 8-1: Compressor Test Loop

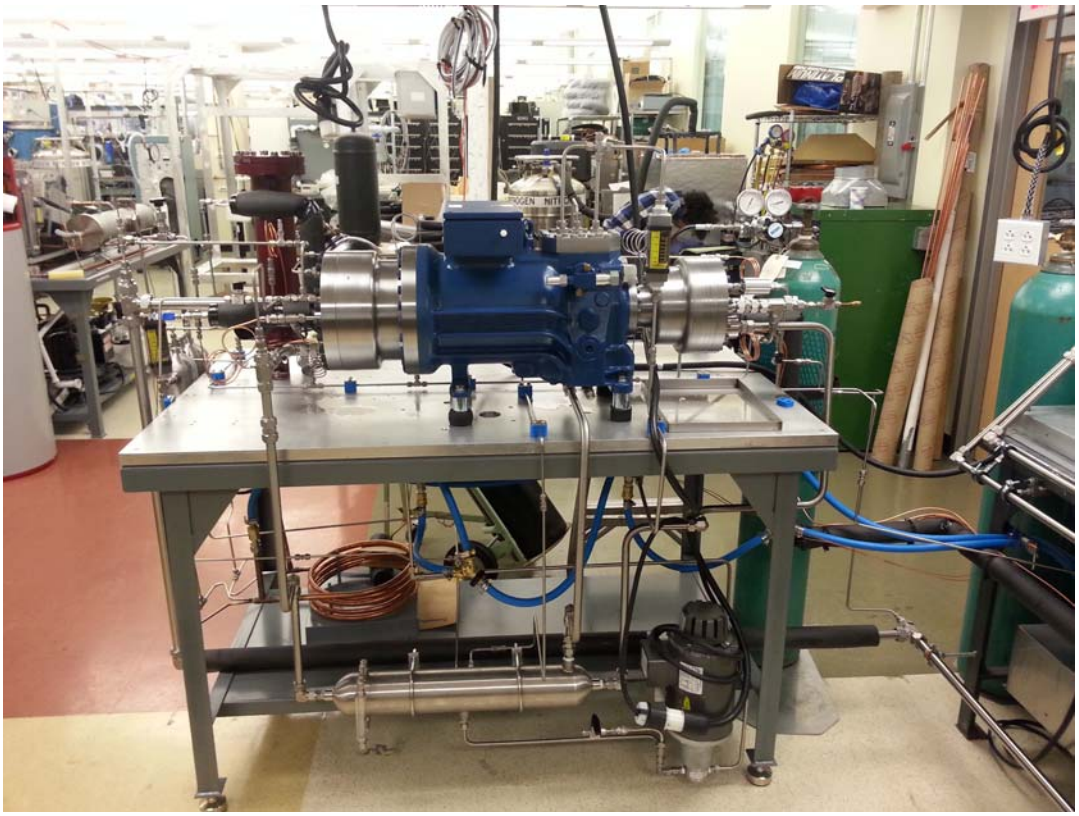

Figure 8-2: Compressor Side of Compressor Test Loop

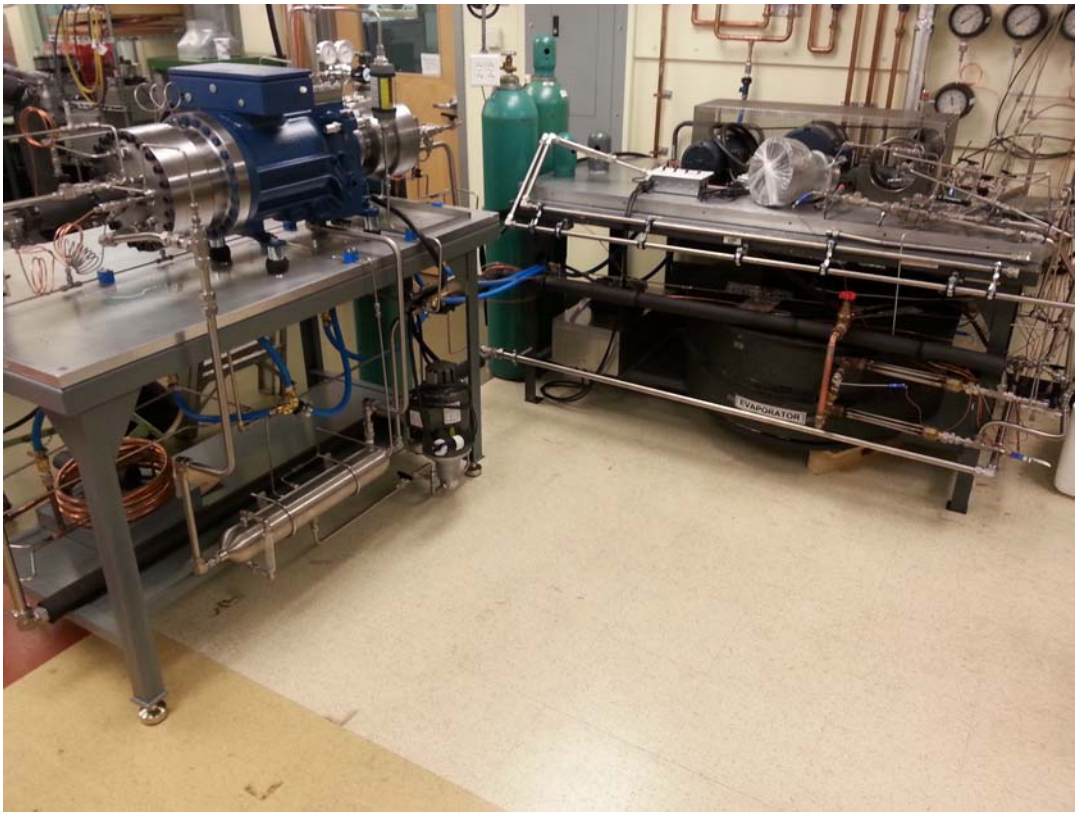

Figure 8-3: Overall Compressor Test Loop

8.2 Test Results

We installed the compressor of the integrated compressor expander into the modified test loop. The modified test loop removed the Dorin CO_2 compressor which had been used to supply pressurized CO_2 to the expander for its testing. The oil was changed from the PAG oil used in the Dorin CO_2 compressor to a POE oil – Fuchs-Reniso C85 oil.

In the initial tests of the compressor, we encountered problems with both oil management and intermediate pressure control, which resulted in surface damage to the scrolls and damage to the Oldham coupling. The scrolls were reworked and the oil management and intermediate pressure control systems were modified and further testing was undertaken.

Table 8-1 gives the results of tests that were run after the above-mentioned modifications were completed. The intermediate (orbital drive) pressure control was adjusted in steps to the point where $P_{intermediate} = 0.44\ P_{low} + 0.56\ P_{high}$ (a small amount higher than the average of the compressor inlet and discharge pressures). The lower part of the table uses the direct test data to calculate the CO_2 mass flow rate, (based on the water side to CO_2 side heat balance in the gas cooler) volumetric efficiency (actual/ideal CO_2 flow), and isentropic efficiency (electric power input to motor basis). The results at 1800 RPM indicate approximately 50% higher than ideal CO_2 mass flow and isentropic efficiency greater than 100%. These impossibilities are attributable to a high oil circulation rate with the CO_2, adding to the thermal load on the gas cooler. With the axially and radially compliant orbital drive and the high oil flow through the compressor scrolls, we expect that the internal leakage between the scrolls would be negligible and the actual volumetric efficiency would be close to 100%. Assuming that the volumetric efficiency was 100%, the isentropic efficiency at the 600 psig/1200 psig, 1800 RPM data points (the right-most two columns of Table 8-1) would be 68% and 69% (electric power input basis), roughly comparable to the isentropic efficiency of state-of-the-art scroll compressors for conventional fluorocarbon refrigerants such as R-410A.

Following the set of test points in Table 8-1, we began to reduce the oil flow to the CO_2 inlet to the scroll compressor. After a brief run time, the same galling failure to the scrolls occurred that had occurred with initial tests.

The damaged scroll surfaces were re-machined, removing approximately 0.010 inch of material, restoring an acceptable surface finish. To reduce the possibility of this kind of destructive, galling axial contact between the two scrolls, a nominal 0.001 inch tip clearance was introduced to allow for thermal expansion and deflection under pressure loading. Calculations indicated that oil present in the scrolls would adequately seal a tip gap this large. With these changes made, the compressor was reassembled and tested again. The test results are in Table 8-2. Excess oil circulation again results in overstated volumetric and isentropic efficiencies, similar to the results in Table 8-1.

Future development efforts will focus on improving the overall oil management system:

- Improved oil separation from the compressor discharge, so that minimal oil circulates through the system
- Optimizing the amount of oil introduced to the scrolls, so that only the amount of oil needed to lubricate and enhance the sealing of the scrolls is introduced to the compressor inlet

Table 8-1: Scroll CO_2 Compressor Test Results

Time - 2/15/2013	3:13	3:38	3:48	4:11	4:27	4:42
Test Notes						
P - Compressor inlet, psig	258	397	405	500	595	595
P - Compressor discharge, psig	608	780	800	1000	1220	1220
P - Gas cooler inlet, psig	614	794	796	1008	1196	1196
P - Evaporator outlet, psig	260	395	410	505	600	600
P - Crank case, psig	460	612	618	760	940	930
P - Oil film, psig	500	680	690	865	1045	1040
T - Compressor inlet, °C	30.1	30.2	31	29.9	29.1	29.1
T - Compressor discharge, °C	87.4	72	68	67	65.1	65.3
T - Gas cooler inlet, °C	80.6	70.6	66.9	65.8	64.3	64.4
T - Gas cooler outlet, °C	29.4	30.2	33	37.8	43.1	42.8
T - Evaporator inlet, °C	1.3	3.2	10.3	11	14.9	14.7
T - Evaporator Outlet, °C	21.3	18.7	22.7	21.6	23.6	24.9
T - Water gas cooler inlet, °C	29.5	29.5	29.6	29.5	29.4	29.7
T - Water gas cooler outlet , °C	33.5	36.5	41	46.7	51.5	51.6
T - Water evaporator outlet, °C	31.2	31.1	32.3	31.7	31.3	31.3
F - Water flow rate gas cooler, gpm	2.5	2.5	2.5	2.5	2.5	2.5
F - Water flow rate evaporator, gpm	1.8	1.8	1.8	1.8	1.8	1.8
Compressor speed, rpm	1200	1200	1800	1800	1800	1800
Compressor power input, kW	3.2	3.7	5.5	6.7	7.9	7.8
Compressor power draw, A	10.4	10.8	10.8	11.9	13.2	13.2
Compressor voltage, V	319	318	472	471	470	470
Oil into compressor, gpm	0.35	0.4	0.4	0.4	0.4	0.4
Oil into bearings, gpm	0.17	0.17	0.17	0.22	0.25	0.25
h - CO_2 gas cooler inlet, kJ/kg	524.6	502.0	497.1	480.1	461.5	461.7
h - CO_2 gas cooler outlet, kJ/kg	461.4	440.8	446.0	424.8	405.0	403.6
h - H_2O gas cooler inlet, kJ/kg	123.7	123.7	124.2	123.7	123.3	124.6
h - H_2O gas cooler outet, kJ/kg	140.5	153.0	171.8	195.6	215.7	216.1
rho - H_2O gas cooler inlet, kg/m^3	995.8	995.8	995.8	995.8	995.8	995.7
mdot - H_2O gas cooler, kg/s	0.157	0.157	0.157	0.157	0.157	0.157
mdot - CO_2, kg/s	0.041567	0.075099	0.146527	0.204142	0.25645	0.247159
rho - CO_2 compressor inlet, kg/m^3	36.2	58.1	59.2	76.7	96.8	96.8
mdot - CO_2 ideal, kg/s	0.041562	0.066684	0.101904	0.132047	0.166507	0.166507
Actual/ideal CO_2 flow	1.00	1.13	1.44	1.55	1.54	1.48
s - CO_2 compressor inlet, kJ/kg-K	2.159	2.055	2.053	1.990	1.931	1.931
h - CO_2 compressor inlet, kJ/kg	492.9	482.4	482.6	473.2	462.9	462.9
h - CO_2 ideal compressor discharge, kJ/kg	540.3	517.8	517.1	507.4	495.1	495.1
h - CO_2 actual compressor discharge, kJ/kg	532.2	503.8	498.5	481.9	463.0	463.4
P - Ideal power consumption, kW	1.97	2.66	5.06	6.98	8.25	7.95
eta - Isentropic efficiency	0.616	0.719	0.920	1.042	1.044	1.020

Table 8-2: Scroll CO_2 Compressor Test Results

Time - 3/18/2013 and 3/19/2013	4:17	4:37	4:52		3:43	3:58	4:10
Test Notes							
P - Compressor inlet, psig	280	385	490		515	625	610
P - Compressor discharge, psig	600	805	995		1035	1220	1320
P - Gas cooler inlet, psig	600	805	995		1035	1231	1300
P - Gas cooler outlet, psig	600	805	995		1035	1234	1338
P - Evaporator inlet, psig							
P - Evaporator outlet, psig	280	385	490		520	630	640
P - Crank case, psig	450	610	770		795	900	1100
P - Oil film, psig	460	660	900		950	1120	1195
T - Compressor inlet, °C	24.9	29.9	31.8		30.5	34.1	37
T - Compressor discharge, °C	65	63.6	61.3		57.5	62.5	69.9
T - Gas cooler inlet, °C	64.2	62.4	61.2		58	62.7	69.8
T - Gas cooler outlet, °C	32	36.8	38.9		40.8	45.7	47.8
T - Evaporator inlet, °C	16.5	18	20		21.8	25	24.2
T - Evaporator Outlet, °C	25.3	25.3	23.8		26	20.4	20.3
T - Water gas cooler inlet, °C	29.8	29.7	29.7		29.8	33	35.2
T - Water gas cooler outlet , °C	37.2	41.3	43.7		44.8	50.6	54.3
T - Water evaporator outlet, °C	33.3	34	34.2		33.5	37.3	39.8
F - Water flow rate gas cooler, gpm	2.4	2.5	2.4		2.3	2.3	2.4
F - Water flow rate evaporator, gpm	1.7	1.8	1.7		1.6	1.6	1.7
F - Oil into bearings, gpm	0.16	0.17	0.19		0.19	0.22	0.22
F - Oil into compressor, gpm	0.7	0.67	0.75		0.6	0.67	0.62
Compressor speed, rpm	1800	1800	1800		1800	1800	1800
Compressor power input, kW	4.8	6.2	6.9		7.3	8.5	9.3
Compressor power draw, A	10	11.2	12.3		12.6	13.9	15.2
Compressor voltage, V	472	472	469		474	474	473
h - CO_2 gas cooler inlet, kJ/kg	506.7	490.6	473.9		465.1	455.0	462.7
h - CO_2 gas cooler outlet, kJ/kg	466.5	451.9	430.1		428.7	408.5	403.0
h - H_2O gas cooler inlet, kJ/kg	125.0	124.6	124.6		125.0	138.4	147.6
h - H_2O gas cooler outet, kJ/kg	155.9	173.0	183.1		187.7	211.9	227.4
rho - H_2O gas cooler inlet, kg/m^3	995.7	995.7	995.7		995.7	994.7	994.0
mdot - H_2O gas cooler, kg/s	0.151	0.157	0.151		0.144	0.144	0.151
mdot - CO_2, kg/s	0.11607	0.197052	0.201328		0.248975	0.228163	0.201276
rho - CO_2 compressor inlet, kg/m^3	40.5	56.2	73.9		79.3	99.4	94.2
mdot - CO_2 ideal, kg/s	0.069707	0.09672	0.127215		0.136474	0.171053	0.162043
Actual/ideal CO_2 flow	1.67	2.04	1.58		1.82	1.33	1.24
s - CO_2 compressor inlet, kJ/kg-K	2.123	2.062	2.004		1.984	1.937	1.958
h - CO_2 compressor inlet, kJ/kg	486.0	483.0	476.4		472.6	467.0	472.3
h - CO_2 ideal compressor discharge, kJ/kg	525.9	521.0	511.6		506.5	498.8	509.3
h - CO_2 actual compressor discharge, kJ/kg	507.6	492.2	474.1		464.2	454.6	462.8
P - Ideal power consumption, kW	4.63	7.49	7.08		8.45	7.27	7.45
eta - Isentropic efficiency	0.965	1.209	1.027		1.157	0.855	0.801

9.0 Conclusions

Design, fabrication, and testing of a scroll CO_2 expander for commercial refrigeration was undertaken and completed. Key performance results were:

- Isentropic expansion efficiency (shaft power output basis) up to 76% was measured.
- At all test conditions and configurations, isentropic efficiency was typically 60% to 65%
- Internal leakage between the scrolls accounted for a significant portion of the observed inefficiency
- The incrementally lower efficiencies (low to mid 60% vs mid 70%) is attributed to suboptimal thrust bearing performance. We have identified a path forward to improve the thrust bearing performance
- The mechanical design is otherwise robust
    - No wear to the scroll sidewalls (a.k.a flanks) occurred, verifying that robust hydrodynamic lubrication was provided by the liquid CO_2 phase in the trailing wedge of the scroll pockets
    - Minimum wear to the scroll tips
    - No wear observed in the oil lubricated bearing surfaces – shaft bearings, orbiting scroll drive bearing, and Oldham coupling

A scroll compressor matching the scroll expander was designed, fabricated, and tested. The hermetic drive motor and housing of a Bock CO_2 compressor was used to drive the compressor. The design provided for integration of the expander. Limited testing of the compressor was done as the program schedule and budget expired. Oil management and thrust bearing performance was in the process of being tuned, but this wasn't completed. The limited test results reported in Section 8 include the effect of large amounts of oil circulating with the CO_2, obscuring CO_2 mass flow measurements (based on the heat balance between the two sides of the gas cooler), and hence capacity and efficiency measurements. Measured input electric power to the compressor drive motor was approximately 25% higher than the isentropic power based on the inlet and outlet pressures and the volumetric capacity (displacement X speed) of the compressor.

Continued work will focus on:

- Reconfiguring the thrust bearings to provide a stiffer net pressure loading – oil film thickness characteristic, enabling the two scrolls to be reliably operated at the closest possible tip clearance
- Improving the oil management configuration to match the bearing oil flow to the compressor scroll inlet oil flow and to minimize circulation though the remainder of the system.
- Completion of integration of the expander, compressor and drive motor

10.0 References

CBBI, 1971, Harry C. Rippel, *Cast Bronze Bearing Design Manual*, Cast Bronze Bearing Institute, Inc.